The Repair Mechanism of Double-Stranded Breaks in Post-Mitotic Neuronal Cells

A thesis
submitted partial fulfilment
of the requirements for the degree
of
MSc (Research)
at
The University of Waikato
by
GRACE CATHERINE-MARY COFFIN

THE UNIVERSITY OF
WAIKATO
Te Whare Wānanga o Waikato

2019

Abstract

A neuron is a fundamental unit of the nervous system. These cells are differentiated and are not readily replaced. They are extremely active and display high metabolic rates. Because of their high activity they are subjected to a large amount of DNA damage throughout their lives. The most genotoxic type of DNA damage is a break in both strands of DNA and there can be as many as 10 to 50 double-stranded breaks (DSBs) in every cell per day. Because of this, a high-fidelity DNA repair mechanism would seem critical for ensuring neuronal longevity.

There are two main mechanisms in which DNA DSBs are repaired: homologous recombination repair (HRR) and non-homologous end joining (NHEJ). HRR is said to occur in proliferating cells, whereas NHEJ is said to occur in post-mitotic cells. HRR is a high-fidelity process that uses a homologous copy of damaged DNA, usually from a sister chromatid, as a template to achieve error-free repair. In contrast, NHEJ is an error-prone system that simply uses a resection/re-ligation method to join the two ends of DNA back together. Because neurons are post-mitotic, they are thought to be repaired by NHEJ. However, given their longevity and high levels of activity, it would seem essential that neurons repair DNA DSBs by an error-free system.

The goal of this study was to determine whether HRR occurs in post-mitotic neuronal cells. The cell line Neuro-2a (N2a) is a mouse derived neuroblastoma cell line. The first objective of this project was to determine a differentiation protocol for this cell line. It was found, through cell counting and EdU incorporation assays, that cells treated with media containing 1% foetal bovine serum (FBS) and 10 μM retinoic acid (RA), over the course of seven days, showed the greatest number of N2a cells entering a non-proliferative state.

The plasmids DR-GFP and I-SceI were amplified and purified by bacterial transformation and miniprep. Once the plasmids were purified, DR-GFP

was transfected into N2a cells by lipofection. The DR-GFP plasmid is a vector that has been engineered to contain a non-functional full-length green fluorescent protein (GFP) gene with a 5'-premature stop codon/*I-SceI* recognition sequence. These transfected cells were then treated with puromycin, as the DR-GFP plasmid contains a puromycin resistance gene, to generate a stable N2a-DRGFP cell line.

Once stable integration of DR-GFP was achieved, the N2a-DRGFP cells were then transfected with the I-SceI plasmid. *I-SceI* restriction endonuclease encoded by the I-SceI plasmid, has no recognition sequence in the mouse genome, so the expression of *I-SceI* will induce a single DSB at the DR-GFP 5'-premature stop codon/*I-SceI* recognition site. The DR-GFP vector contains a portion of the wild-type GFP sequence, so if HRR occurs after *I-SceI* expression, the GFP 5'- premature stop codon will be removed and a functional GFP protein will be detected by immunofluorescence.

No fluorescence was observed after *I-SceI* transfection in proliferating cells. PCR amplification of a DR-GFP sequence from N2a-DRGFP cells showed that DR-GFP had not been stably integrated into N2a cells. Similarly, co-transfection of I-SceI and DR-GFP into N2a cells also did not show any fluorescence. To determine possible causes for this result, plasmids were sequenced, and it was found that the DR-GFP sequence was incorrect. Because of this, no further experimentation of HRR in post-mitotic cells could occur until the correct DR-GFP plasmid is obtained.

Acknowledgements

I would like to thank Associate Professor Brett Langley for your help and guidance. You have taught me so much over the past year and I have gained so much more knowledge about scientific processes, both in the laboratory and with the writing method. Thank you for your support throughout the year, I really appreciate all you that you have done.

To my parents, thank you for all your love and support over the years. You have been a wonderful support system and have helped me become the person I am today.

And to Bradley, thank you so much for making every day a little bit easier. You believed in me even when I didn't believe in myself and have always been supportive of my goals. I truly do appreciate everything you have done for me.

Table of Contents

List of Figures

List of Tables

Abbreviations

53BP1 = p53-binding protein

AD = Alzheimer's disease

ALS = Amyotrophic lateral sclerosis

Alt-NHEJ = Alternative non-homologous end joining

APP = Amyloid precursor protein

A-T = Ataxia-telangiectasia

ATLD = Ataxia-telangiectasia-like disorder

ATM = Ataxia telangiectasia mutated

BER = Base excision repair

Bp = Base pair

BRCA1 = Breast Cancer 1, early onset

BSA = Bovine serum albumin

CNS = Central nervous system

DAPI = 4′,6-diamidino-2-phenylindole

DDR = DNA damage response

dH_2O = distilled water

DNA = Deoxyribonucleic acid

DNA-PKcs = DNA-dependent protein kinase, catalytic subunit

DSB = Double-stranded break

DSBR = Double-strand break repair

EdU = 5-ethynyl-2'-deoxyuridine

fALS = Familial ALS

FBS = Foetal bovine serum

GFP = Green fluorescent protein

H3K4me3 = Histone 3, lysine 4, tri-methylated

H3K56 = Histone 3, lysine 56

H3K79 = Histone 3, lysine 79

H3K9 = Histone 3, lysine 9

H4K16 = histone 4, lysine 16

H4K20 = Histone 4, lysine 20

H4K20me1 = Histone 4, lysine 20, mono-methylated

H4K20me2 = Histone 4, lysine 20, di-methylated

H4K20me3 = Histone 4, lysine 20, tri-methylated

HAT = Histone acetyltransferase

HDAC = Histone deacetylase

HDM = Histone demethylase

HMT = Histone methyltransferase

HR = Homologous recombination

Kb = Kilobase

MMEJ = Microhomology-mediated end joining

MMR = Mismatch repair

MRN = Mre11-Rad50-Nbs-1

N2a = Neuro2a

NAD+ = Nicotinamide adenine dinucleotide

NBS = Nijmegen break syndrome

NBSLD = Nijmegen break syndrome-like disorder

NER = Nucleotide excision repair

NFT = Neuro fibrillary tangles

NHEJ = Non-homologous end joining

NuRD = Nucleosome remodeling deacetylase

ORF = Open reading frame

PARP = Poly (ADP-ribose) polymerase

PBS = Phosphate buffered saline

PCR = Polymerase chain reaction

PD = Parkinson's disease

PI-3K = Phosphoinositide 3-kinases

PNS = Peripheral nervous system

PolyADP-ribosylation = PARylation

PP2A = protein phosphatase 2A

PTM = Post-translational modification

RA = Retinoic acid

RNA = Ribonucleic acid

RPA = Replication protein A

S139 = Serine 139

sALS= Sporadic ALS

SAM = S-adenosylmethionine

SOD1 = Superoxide dismutase 1

SSB = Single-stranded break

SSBR = Single-strand break repair

ssDNA = Single-stranded DNA

UV light = Ultraviolet light

V(D)J = Variable, diversity, and joining

WS = Werner syndrome

XLF = XRCC4-like factor

XRCC4 = X-ray repair cross-complementing protein 4

Y142 = Tyrosine 142

γH2A.X = Phosphorylated H2A.X

Chapter 1

Literature Review

1.1 Neurons

A neuron is the fundamental unit of the brain and nervous system. It is composed of a cell body or soma, a nucleus, dendrites, an axon, axon terminals, and a myelin sheath (Figure 1.1). Dendrites receive messages in the form of electrochemical signals, which can be either inhibitory or excitatory [1]. The signals received by dendrites are sent to the soma, where the summation of these signals can either equate to an inhibitory or excitatory response [1]. An action potential is an excitatory response and it carries an electrical signal through the axon by depolarisation [2]. Depolarisation occurs due to the movement of sodium and potassium ions through gated ion channels [2]. To assist in the conduction of the electrical signal, specialised cells – Schwann cells in the peripheral nervous system (PNS) and oligodendrocytes in the central nervous system (CNS) – can wrap the axon with myelin. Polarity changes can thus occur at gaps within the myelination, called Nodes of Ranvier, as opposed to the whole axon, which allows faster and more efficient conduction of the action potential than occurs in unmyelinated axons [3]. At the distal end of the axon, the axon terminal, is capable of transmitting signals to other neurons [4]. Here, electrical signals conveyed by the axon are converted to chemical signals, in the form of neurotransmitters [4]. Neurons are connected by synapses, in which there is a small gap called a synaptic cleft where neurotransmitters diffuse across to allow the dendrites of post-synaptic neurons to receive the signal [4].

There are trillions of neurons in a human body, which form networks that communicate to each other with this form of electrochemical signalling to elicit responses. These networks are very intricate and can sometimes be very complex and create the nervous system. The nervous system can be divided into the CNS, which consists of the brain and spinal cord, and the

PNS, which consists of all other nerves in the body. The CNS and PNS communicate with each other to send signals either through an efferent or afferent system [5]. The efferent system is the CNS sending signals to the body and controls two systems; the autonomic and somatic systems. The autonomic system controls involuntary muscles and systems such as breathing and digestion, whereas the somatic system controls voluntary movements such as waving and running. The afferent system sends sensory signals to the CNS from the body such as smell, taste, sound, pain, and touch.

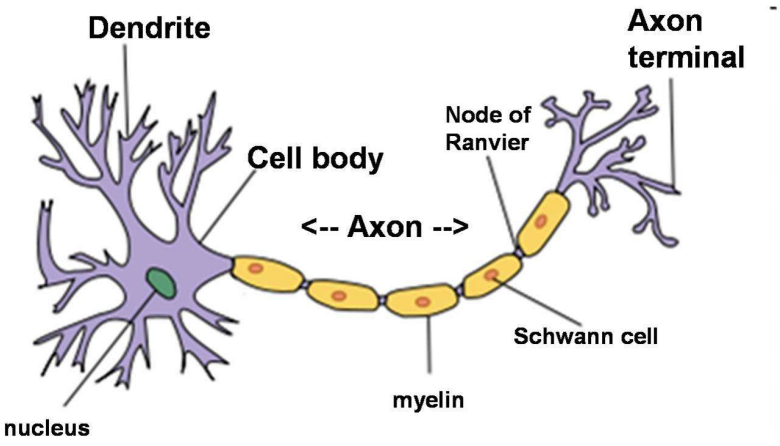

Figure 1.1 Labelled illustration of a neuronal cell [6]

Neurons are highly metabolically active cells and because of this they are can sustain a large amount of DNA damage on a daily basis.

1.2 DNA Damage

There are different types of DNA damage that can occur in cells (Figure 1.2). These include single-base damage, modifications that distort the DNA double-helix, single-stranded breaks (SSBs), and double-stranded breaks (DSBs) [7]. Each form of DNA damage affects the integrity of the DNA, and therefore the cell, in a different way. DNA damage occurs by both endogenous and exogenous sources [7].

DNA damage can arise from endogenous sources, such as metabolic processes that can create reactive oxygen or nitrogen species. For example, processes of mitochondrial respiration, DNA replication, DNA transcription, and V(D)J recombination that occurs in lymphocytes [8-10]. Reactive oxygen and nitrogen species are one of the main causes of DNA damage in the brain due to its high metabolic activity [7]. Exposure to UV light, ionising radiation, and chemotherapy agents are exogenous causes of DNA damage [7]. If damage is left unrepaired it can affect the integrity of the genome [11].

A bulky DNA adduct is where a segment of DNA is bound to a cancer-causing chemical and are caused by exposure to polycyclic aromatic hydrocarbons (PAHs) [12]. If this damage is not repaired effectively, it can potentially lead to carcinogenesis [13].

Intra-strand and inter-strand crosslinks can also occur in DNA. Endogenous and exogenous agents can react with nucleotides and cause covalent bonds to be formed either on the same strand of DNA (intra-strand crosslinking) or on opposite strands of DNA (inter-strand crosslinking) [14]. Inter-strand crosslinking is particularly toxic as it prevents transcription and replication by inhibiting strand separation [14], and can lead to a DSB.

Single base damage is formed when a nucleotide within DNA is chemically damaged, which can be due to oxidation, alkylation, or deamination [15]. In addition, the nucleotide uracil can be inappropriately incorporated into DNA [15]. If single-base damage is not repaired, it can lead to a SSB in the DNA.

Single-strand breaks are lesions that are formed in one strand of the DNA duplex. Single-strand breaks are the most common type of lesion that arises in cells [16]. This damage can cause an altered nucleotide sequence of the damaged DNA and can also lead to DSBs, which can affect the integrity of the cell if not repaired [17].

Double-strand breaks are the most genotoxic of all DNA damage [18]. DSBs are lesions that are formed when both strands of the DNA duplex are broken, and if not repaired, can cause apoptosis of the cell. If misrepaired, they can cause a loss of genetic information, mutations, and chromosomal rearrangement [7, 8, 11, 18, 19]. The main endogenous cause of DSBs is when a DNA replication fork encounters an unrepaired DNA lesion, which triggers the collapse of the fork [20].

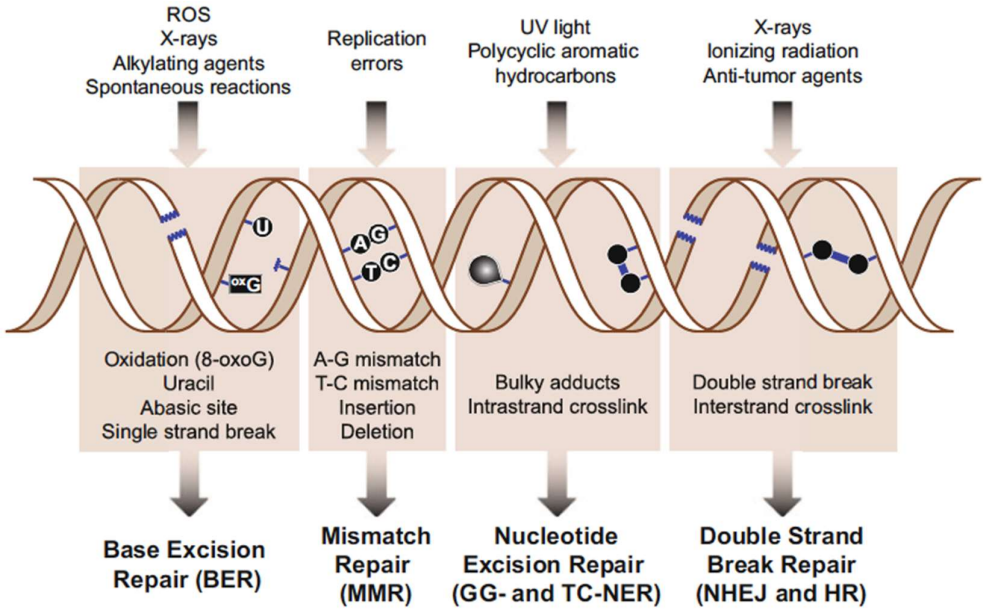

Figure 1.2 Types of DNA damage [21]

Because DNA damage can affect the genome in such a crucial way, DNA repair pathways are essential to protect the integrity of the cell.

1.3 DNA Repair Mechanisms

Because there is a wide variety of DNA damage that can occur, there are many DNA repair pathways, each with overlapping or different complexes and factors involved. The base excision repair (BER) pathway is responsible for repairing single base damage that does not distort the DNA helix [22]. The downstream steps of BER are also responsible for the repair of SSBs. The nucleotide excision (NER) pathway is responsible for repairing bulky lesions that distort the DNA helix [23]. DNA mismatch repair (MMR) pathway

is responsible for repairing insertions, deletions, and mis-incorporation of bases that can arise during DNA replication and recombination [24]. The double-strand break repair (DSBR) pathway is responsible for repairing double-strand breaks and inter-strand crosslinks [7]. DSBR pathways are crucial in a cell because the consequences that occur if a DSB is not repaired or misrepaired can be catastrophic.

1.3.1 Double-Strand Break Response

When a DSB occurs, a response is activated almost instantly, which is called the DSB response. The DSB response is a multi-tiered process that involves the rapid recruitment of “sensors” to the break site. H2AX is sensor and is a histone variant of the protein family H2A. H2AX is rapidly phosphorylated to form γH2AX following DNA damage. The phosphorylation of H2AX creates a euchromatin structure surrounding the break site which allows access to repair factors and checkpoint proteins [25]. The MRN complex (Mre11, RAD50, and Nbs1) is also a sensor and processes the free DNA ends after DNA damage and creates a signal cascade that activates “transducers” [26, 27]. Ataxia telangiectasia mutated (ATM) and DNA-dependent protein kinase, catalytic subunit (DNA-PKcs), are transducers that amplify signals to downstream effectors that are associated with DNA repair and are regulated by mediator proteins [8, 19, 28]. There are two mediator proteins and their affinity to bind at the DSB determines the pathway that will be used to repair the DNA damage [29].

1.3.2 Homologous Recombination and Non-Homologous End Joining

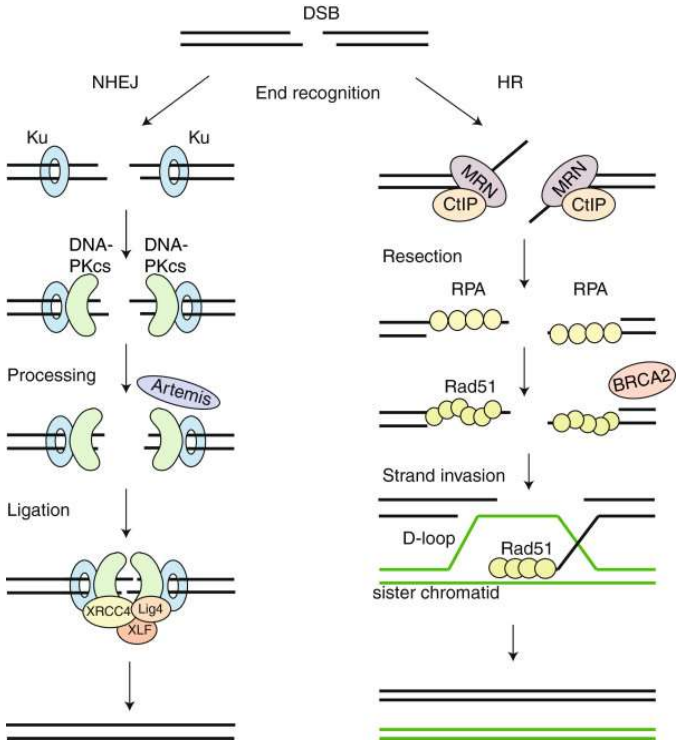

Figure 1.3 DSB repair pathways

The two main mechanisms by which DSBs are repaired are homologous recombination repair (HRR) and non-homologous end joining (NHEJ) pathways [7, 11] (Figure 1.3). There is also an alternative pathway by which DSBs can be repaired called microhomology-mediated end joining (MMEJ) or alternative NHEJ (alt-NHEJ) [30]. The mechanism of this pathway is still actively being researched, but it uses micro-homologous sequences and is kinetically much slower than the classic NHEJ pathway [30]. This pathway is very error prone and often results in deletions, translocations, complex rearrangements and inversions [31].

HRR is a complex, energy consuming but high-fidelity process based on homologous recombination where a homologous copy of the sequence, for example a sister chromatid, is used as a template to achieve error-free repair [32]. HRR requires DNA processing to occur at the DNA DSB site via

the MRN complex and CtIP. The MRN-CtIP complex resects DNA and generates a 3' single stranded DNA (ssDNA). This ssDNA is then coated by Replication protein A (RPA), which removes the secondary structure [33]. BRCA2 then mediates the replacement of RPA with RAD51. Once RAD51 is assembled it forms a nucleoprotein filament and promotes a search for a homologous sequence to use as a template for repair. Rad52, Rad54, and Rad51 paralogs (Xrcc2, Xrcc3, Rad51L2, Rad51L3) are also recruited to the lesion to facilitate strand invasion and recombination. After strand invasion and formation of the D-loop, the DNA end is extended using the homologous sequence as a template [34]. Both ends of the DSB are engaged and this can be by either independent strand invasion or by second end capture, which leads to double Holliday junction formation. The junction can be processed by a resolvase into non-crossover or crossover products [35].

NHEJ is a very simple system in comparison to HRR and can occur at any phase in the cell cycle but predominates in the G1 and G2 phase [7, 36, 37]. It functions by the use of a resection/re-ligation mechanism to put the two ends of DNA back together [7, 36, 37]. This is a very error-prone system, and crucial information can be lost due to small insertions, deletions, substitutions at the break site, and translocations if DSBs from differing parts of the genome are joined together [11, 36]. NHEJ is mediated by Ku70/Ku80 heterodimer, which forms a ring around the DNA DSB site [38]. Ku70/Ku80 then allows the recruitment of the DNA-PKcs. If the DNA ends are not able to be directly ligated the nucleases Artemis or Exo1 will then process the damaged DNA, and the DNA polymerases Polλ and Polμ will fill the gap [39]. When the DNA ends are matched, DNA ligase IV and cofactor Xrcc4 will mediate their ligation [40].

HRR is believed to occur in proliferating cells, whereas NHEJ repair is believed to occur in post-mitotic cells [7, 11, 18]. HRR is a complex system that occurs in the S and G2/M phase of the cell cycle and uses a homologous copy of the DNA sequence, such as a sister chromatid, as a template to achieve error-free repair of the DSB [7]. This system is very

effective, but is energy and time-consuming; it takes hours to repair these breaks, compared to only 30 minutes in NHEJ [37].

The utilisation of a high-fidelity repair process such as HRR in proliferating cells makes sense as an error-prone system of repair could lead to a clonal expansion of a misrepaired genome if the DNA damage is not repaired accurately. In contrast, in post-mitotic cells, which do not divide, an error-free repair process is thought to be less critical and NHEJ repair is sufficient; if the repair of the DSB introduces a deleterious mutation, the potentially expendable cell can be deleted through a process such as apoptosis without affecting the organism or future generations of cells.

Because there is such a vast number of neurons in the human body and the networks which they form are extremely active [19], neurons are subjected to large amounts of DNA damage; up to 50 DSBs per cell per day have been reported [41]. Neurons are post-mitotic cells, so loss of these cells due to DNA damage can be very consequential. If DNA damage is left to accumulate it can cause DNA lesions, which in proliferating cells can lead to cancer, whereas in neurons it can lead to neurodegenerative pathologies [42]. Because it is crucial that neurons last for a life time, it would make sense for a higher fidelity repair process such as HRR to occur in these cells to maintain their integrity.

1.3.3 Pathway Choice

Pathway choice for a DSB is determined by mediator proteins and they differ between HRR and NHEJ. The affinity that these proteins have to the DNA break site determines which pathway will be selected for in the repair of DSBs [37]. The HRR pathway is mediated by Breast Cancer 1, early onset (BRCA1), while NHEJ is mediated by p53-binding protein (53BP1). There is a balance between these two mediators and their binding affinities affect each other. 53BP1 has been identified as a negative regulator of HRR as it limits the resection of DSBs and steers the repair towards the NHEJ pathway [37, 43]. The resection of a DNA DSB is a negative regulator of the

NHEJ pathway as the processing guides the repair pathway towards HRR and prevents the binding of NHEJ repair factors [43].

Post-translational modifications (PTMs) play a prominent role in the binding affinity of these mediators and determines whether HRR or NHEJ mechanisms are used for the repair of DNA DSBs [8]. PTMs are also involved in many other aspects of the DSBR.

1.4 Post-Translational Modifications

Histones are a family of positively charged proteins that assist with packing negatively charged DNA into a condensed chromatin structure that allows DNA to fit into the nucleus of a cell. Nucleosomes are the basic subunit of chromatin and are comprised of approximately 146 bp of DNA wrapped around an octameric histone core, which is formed by histones H2A, H2B, H3, and H4.

Histone modifications in the form of PTMs assist in the response to DNA damage. PTMs can occur on the C- or N- terminals of the histone tails. There are many types of PTMs that can occur in histones including: acetylation, methylation, phosphorylation, ubiquitination, and PolyADP-ribosylation [8, 44]. These modifications can affect the DSB response at different phases which include: the detection of DSBs; the restoration of chromatin back to its condensed state once the DNA has been repaired; the regulation and accessibility of chromatin for repair factors and the binding of checkpoint proteins; and the activation of checkpoint signals [8].

1.4.1 Acetylation

Histone acetyltransferases (HATs) add acetyl groups to histone tails, whereas histone deacetylases (HDACs) remove acetyl groups from histone tails. HATs and HDACs play an important role in the accessibility of chromatin to binding factors once DNA damage is detected.

It has been shown that acetylation of the histone H4K16 in chromatin surrounding the double-strand break-site inhibits the NHEJ pathway as it decreases the binding affinity of 53BP1 [45]. This allows for the binding of BRCA1 to the break-site which promotes HRR [45]. The acetylation of H4K16 allows for the regulation of the two pathways by controlling the binding affinity of mediators to the DNA break-site.

The acetylation of lysine 56 on histone H3 (H3K56) occurs in high numbers in newly synthesised histone H3 molecules following the S phase of the cell cycle [46-48]. The acetylation of H3K56 declines throughout the cell cycle and is very low during the G2 phase; however, in the presence of DNA damage, acetylation of H3K56 remains high, which suggests that it is important in the DNA damage response [46-48]. The acetylation of H3K56 creates a favourable environment for DNA repair as it allows access to DNA repair machinery by the relaxation of chromatin [46-50].

HDAC1 and HDAC2 are rapidly recruited to DNA damage sites where they deacetylase H4K16 and H3K56 [8, 51]. The deacetylation of H4K16 is important for repair via the NHEJ pathway, as it prevents BRCA1 from binding to the break site, and deficiency in HDAC1 and HDAC2 activity results in defective repair by NHEJ [51].

1.4.2 Phosphorylation

H2AX is a member of the histone H2A family. Phosphorylation of serine 139 (S139) on H2AX plays an important role in the response to DNA damage. Within seconds of DNA damage, S139 on H2AX surrounding the DSB site is phosphorylated, followed by those further away from the break site (up to 2 mb) [46]. The levels of phosphorylated H2AX (γH2AX) are reflective of the total DSBs within a cell. The phosphorylation of H2AX creates a euchromatin structure surrounding the break site, which allows access to repair factors and checkpoint proteins [25]. This allows the DNA DSBs to be either repaired or leads the damaged cell being directed towards an apoptotic pathway.

ATM and DNA-PKcs are responsible for the phosphorylation of H2AX. These proteins are both part of the phosphoinositide 3-kinases (PI-3Ks) family and they act to repair damage. ATM and DNA-PKcs sense and bind to the DNA break site, which leads to their activation and the subsequent phosphorylation of H2AX around the break site [52, 53]. Histone H2AX is also dephosphorylated at tyrosine 142 (H2AX Y142) and is important for the formation maintenance of γH2AX at the site of the DSB [25]. It also acts to recruit repair factors for the repair of the DSB [54, 55]. After the DSB is repaired it is important for the removal of γH2AX to condense the chromatin once again. This can be achieved by γH2AX being removed from chromatin by histone exchange or dephosphorylated by protein phosphatase 2A (PP2A) [56].

1.4.3 Ubiquitination

The E3 ubiquitin ligases, RNF8 and RNF168, play a key role in the promotion and accumulation of DNA repair factors to the DNA DSB site [57]. RNF8 and RNF168 ubiquitylate specific marks on histone H2A, which is essential for DSB repair [57] .

When H2AX is phosphorylated it allows for MDC1 protein to bind to the DNA break site [58]. MDC1 acts as a scaffold protein that recruits other DNA repair factors to the site of DNA damage [58, 59]. This includes RNF8 and RNF168. This binding allows RNF8 and RNF168 to ubiquitylate marks on histone H2A, near the DSB site [60]. These ubiquitin marks allow further proteins and factors associated with the damage response to bind and help repair DNA damage [60].

1.4.4 Methylation

Histone methyltransferases (HMTs) are responsible for the transfer of methyl- groups from S-adenosylmethionine (SAM) to histones. Histone demethylases (HDMs) are responsible for the removal of these methyl groups from histones. Components of histones H3 and H4 are known to be

methylated in response to DNA damage. Lysine residues on histones H3 and H4 can be either mono-, di- or tri- methylated (me1, me2, me3, respectively) in response to DNA damage.

Methylation of lysine 20 of histone H4 (H4K20) is known to be involved in the DNA damage response. H4K20me1 and H4K20me2 are involved with DNA replication and DNA damage repair, whereas H4K20me3 is associated with the silencing of the heterochromatic region [61]. H4K20 is always in a methylated state but it is not often detected due to the heterochromatin structure of a cell when it is not stressed. However, in a stressed state the chromatin is loosened, thus the methylation mark can be detected. Mono- and di-methylated H4K20 allows 53BP1 to bind to the site of the damage [62].

Methylated lysine 79 of histone H3 (H3K79) is another example of a histone protein that is always in a methylated state but is not detected due to the heterochromatic structure of the chromatin in an unstressed cell. When the cell becomes stressed and the chromatin is loosened, this methylation mark can be detected and allows 53BP1 to be recruited [63]. 53BP1 is the mediator for the NHEJ pathway, so H4K20 and H3K79 are both positive regulators of the NHEJ pathway. These proteins work together to ensure that 53BP1 is recruited to the break site [63].

1.4.5 Poly ADP-Ribosylation

PolyADP-ribosylation (PARylation) regulates DNA repair, chromatin organisation, transcription, and replication. It is the process in which polymers of ADP-ribose are transferred from the co-substrate nictonamide adenine dinucleotide (NAD+) to proteins that have specific amino acid side chains that can accept the ADP-ribose moiety. Enzymes called poly (ADP-ribose) polymerase (PARP) are responsible for this transfer.

PARP-1 is the most abundant PARP family member and it is involved in DSB response. After a DNA DSB there is rapid PARylation of the chromatin.

This allows for recruitment of chromatin remodelling factors, such as NuRD and ALC1, which are essential for the DNA repair process [64].

PARP-1 can also function as an alternative pathway to the NHEJ pathway. PARP-1 can bind directly to DNA and compete with Ku [65]. However, Ku has a higher binding affinity to damaged DNA, so will preferentially bind to DNA DSBs. PARP-1 is a back-up repair pathway to the NHEJ pathway, if the repair factors for NHEJ are not available [65].

1.4.6 Summary of Post-Translational Modifications

The PTMs that occur in neurons following a DSB are essential, as they restructure the chromatin, and recruit repair factors and checkpoint proteins, to repair the DNA damage. This response happens within seconds to minutes of DNA damage and leads to proficient repair of DNA damage.

PTMs also play an important role in determining which DNA DSB repair pathway will be used, and thus determines the accuracy in which a DSB is repaired. The predominant PTM that determines the pathway is the acetylation of H4K16. Acetylation of H4K16 allows BRCA1 to bind to H4K16 instead of 53BP1, which leads to the resection of the DSB and the HRR pathway is used.

1.5 DNA Repair in Neurons

The repair of DNA damage, especially DNA DSBs is essential in an organism, as unrepaired or misrepaired DSBs can affect the integrity of the genome and could potentially lead to neurodegenerative pathologies.

The cell cycle plays a role in the repair pathway used. In the S and G2/M phase of the cell cycle, a homologous sequence available in the form of a sister chromatid, making HRR possible. Post-mitotic cells are either in the G0 or G1 phase of the cell cycle, where a homologous sequence is not readily available, so it is thought that HRR cannot occur.

Neurons are different to normal post-mitotic cells in the fact that they are not expendable cells. As such, the accumulation of lesions or deletion of cells due to insufficient DNA repair can lead to neurodegenerative pathologies. NHEJ is associated with the loss of crucial information due to small insertions, deletions, substitutions, and translocations at break sites [11, 36]. If neurons were to repair DSBs primarily by NHEJ it would be expected that DNA damage accumulation and deletion of cells would occur frequently. However, neurodegenerative diseases mainly affect the older population, with only a number of rare cases being early onset. Defective DDRs have been observed in neurodegenerative diseases. Neural defects show the importance of a functioning DDR and how defects in these pathways results in a wide range of disorders.

Neurons do not need to repair themselves quickly for their short-term survival, but it is essential that they have a capacity to repair DNA damage to a sufficient level for long-term survival [19]. Neurons are critical cells in our body, and DNA lesions, if left to accumulate, can lead to neurodegeneration. It would make sense that a high-fidelity repair such as HRR would occur to protect the integrity of these cells.

1.6 Neurodegenerative Diseases

Evidence for neurons maintaining the capacity for high-fidelity repair come from investigations of neurodegenerative disease and injury. The loss of neurons or accumulation of DNA lesions due to an inefficient or defective DDR can lead to a range of neurodegenerative diseases that cause problems with movement (ataxia) and mental functioning (dementia). These diseases are progressive in nature and do not have any known cures.

1.6.1 Aging

Aging is a major risk factor for neurodegeneration [66]. Neurons have extremely high activity, and as a consequence high rates of oxidative damage can occur. Oxidative damage is a major contributor to the degeneration that is observed in both acute and chronic neurodegenerative

disorders [8]. The “Free Radical Theory of Aging” hypothesises centres on oxidative damage, which, if left unrepaired, will contribute to the decline of cellular activities and age-related deterioration [67]. Deficiencies in the repair of DNA damage have been shown to increase with age, and this increase has been correlated with cognitive decline and neurodegeneration that is observed in the aged population [68]. It has also been found that the different brain regions accumulate DNA damage at differing rates, with the most damage in the brain being accumulated in the hippocampus and the cortex [8, 19]. This evidence is consistent with the cognitive and memory decline that is seen in neurodegenerative disorders.

Some insights into the genetics of aging comes from progeroid syndromes, which include, but are not limited to, Werner Syndrome, Bloom syndrome, Xeroderma Pigmentosum, and Cockayne syndrome.

Werner syndrome is one of the most studied progeroid syndromes as it mimics natural aging, but in a much shorter timeframe. It is an autosomal recessive disorder and results from mutation in the WRN protein, a RecQ helicase, which is involved in both NHEJ and HRR pathways. WRN interacts with the Ku70/80, DNA-PKcs, XRCC4 and DNA ligase IV proteins involved in NHEJ [69-71] and with NBS1, which is a part of the MRN complex that is involved in HRR [72]. Mutation may result in truncation of WRN, and a reduction in DNA repair [73]. There is also a down-regulation of the p53 checkpoint protein, that results in a loss of p53-dependent apoptosis, which means that dysfunctional cells will have a higher survival rate [74]. These mutations contribute to the phenotypes observed in WS, which include; wrinkling of skin, skin atrophy, growth retardation, greying of hair, hair loss, prematurely aged faces, loss of fat tissue, and premature aging of the brain [75, 76].

There have been some epigenetic marks that have been linked with the process of aging. The dysregulation of the acetylation of H4K16, which is important for the HRR pathway, has shown to be involved in the aging process in mice, as this dysregulation is associated with memory decline

and deficiency in the DNA repair process [77, 78]. γH2AX, the marker for unrepaired DNA damage, can be used to observe aging. There are two types of γH2AX that can be found in cells and these are: transient γH2AX foci, and residual γH2AX foci [79]. Transient γH2AX are associated with the fast and efficient repair of DNA DSBs, which usually occurs within minutes to hours from the occurrence of the DSB [79]. Residual γH2AX on the other hand, usually can persist for months to years after the occurrence of a DSB and this can be for one of two reasons; either the DSB is slow to repair, or the DSB will remain permanently unrepaired due to either cellular senescence, apoptosis, or because the DSB is on part of the genome that cannot be repaired, such as on telomeres [79-83]. γH2AX and its accumulation due to unrepaired DNA damage has been implicated in diseases that have accelerated aging, such as Werner's syndrome, and Alzheimer's disease [84, 85].

1.6.2 Alzheimer's Disease

Alzheimer's disease (AD) is the most common progressive neurodegenerative disorder, characterised by severe dementia. It mainly affects those over 65 years of age, with 90-95% of those diagnosed being in this age range [86]. The symptoms of AD include memory loss, cognitive decline, and behavioural changes [87]. The later stages of AD also include symptoms of reduced co-ordination and mobility, and tremors [87]. Neuropathologically, patients exhibit extracellular senile plaques that consist of amyloid-β peptide, intra-neuronal neuro fibrillary tangles (NFT), degeneration of synapses, and neuronal cell death [86, 87].

In 1990, it was first shown that DNA strand breaks can be increased by 2-fold in the brain of AD patients compared to controls [88]. In AD patients, there is an observed increase in DSBs and a decrease in DSBR proteins, such as DNA-PKcs and the MRN complex [89, 90]. Recently, it has been shown in mice that are transgenic for human APP – a model for AD – have an increased number of neuronal DSBs compared to that of control mice at

baseline, and there are further increases of DSBs in these transgenic mice when exploring a novel environment [91].

1.6.3 Parkinson's Disease

Parkinson's disease (PD) is a sporadic, progressive, neurodegenerative disease characterized by loss of dopaminergic neurons in the substantia nigra. PD affects motor function, with symptoms including tremors, bradykinesia, and stiffness [92]. The mechanisms of cell death in PD are not well understood, but DNA damage has been implicated with this disease. In a study using post-mortem brains from 5 confirmed cases of PD and 6 age-matched controls, DNA from PD brains showed that the midbrain, caudate nucleus/putamen, thalamus, and hippocampus had more DNA DSBs than healthy aged-matched controls [93].

1.6.4 Amyotrophic Lateral Sclerosis

Amyotrophic Lateral Sclerosis (ALS) is a neurodegenerative disorder that affects motor neurons, which are responsible for voluntary movement. It affects mainly those between the ages of 55-75 years. The upper and lower motor neurons both begin to degenerate and die, which leads to the symptoms observed [94-96]. Symptoms are progressive: at first muscles begin to weaken until they start to atrophy, and patients eventually lose control over their muscles, which makes it almost impossible to walk, talk, eat, and eventually breathe. Patients often die within five years of the symptoms occurring, often from respiratory failure [95].

There are two types of ALS that are observed, familial ALS (fALS), which accounts for up to 10% of cases observed, and sporadic ALS (sALS), which accounts for 90% or more of cases observed [97]. The exact mechanisms in which the degeneration of the motor neurons that is observed in ALS are not known. However, around 20% of all fALS cases are caused by a mutation in copper-zinc superoxide dismutase 1 (SOD1) [97]. Both SSBs and DSBs were detected in motor neurons of transgenic mice for the human mutant SOD1 gene, and the amount of DSBs increased with age [98].

The studies of the motor cortex in post-mortem brains of ALS patients showed that there was an increase of oxidative DNA damage repair activity [99]. DNA damage was suggested to occur upstream of the motor neuron degeneration that occurs in this disease.

1.6.5 Summary of Neurodegenerative Diseases

As can be seen from these examples, with neuropathological conditions, neurons accumulate greater amounts of DNA damage. There is also evidence that non-repaired or misrepaired DNA DSBs contributing to the neurodegenerative pathologies that have been stated in this section.

1.7 Neurological Defects with DNA Repair Mutations

Evidence for neurons maintaining a high-fidelity mechanism of repair also comes from investigations into mutant DNA repair proteins – in all known conditions in which a DNA repair protein is dysfunctional (and not embryonic lethal), a neurological phenotype is present.

Defects due to mutant DNA repair proteins are early onset and are often progressive in nature. These defects play an important role in determining the key factors involved in the DDR and the role that they play.

1.7.1 Ataxia-Telangiectasia

Ataxia-telangiectasia (A-T) is a monogenic disease that is caused due to mutation in the ATM gene [100]. This mutation causes the inactivation or the loss of the gene [101]. ATM is present throughout the DNA damage response, by phosphorylating key proteins, which can lead to either DNA repair or apoptosis of the damaged cell [26]. Because ATM is diverse in its functionality, the loss or inactivation of this protein causes many different phenotypes which include: ataxia, telangiectasia, radiosensitivity, susceptibility to cancer (lymphatic cancer accounts for 80% of cancer

associated with disease [102]), immunodeficiency, and chromosomal translocations [101].

A-T is an early onset, progressive, neurodegenerative disorder. Infants appear normal, but at two to three years of age, ataxia begins to appear and commonly progresses to the child being wheelchair bound by the age of 8 to 12 [101, 103]. By MRI, the cerebellum of patients often appears normal following diagnosis with A-T, but declines in mass significantly by the age of 10 [101]. Because A-T patients are immunodeficient and have a susceptibility to cancer, they have a significantly shortened lifespan, with the percent of survival of those who have A-T rapidly declining to only a very small percentage by the time they reach thirty years old [104]. Similarly, ATM knock-out mice show ataxia, growth retardation, immunodeficiency, meiotic failure, and predisposition to cancer [105], similar to that of ATM in humans.

1.7.2 Ataxia-Telangiectasia-Like Disorder

Ataxia-telangiectasia-like disorder (ATLD) is a very rare disorder, which shares many similarities with A-T. ATLD is caused by a hypomorphic mutation in the MRE11 gene, which results in a deficiency of the MRE11 protein, with the protein either truncated or full-length and mutant [106, 107]. MRE11 complexes with RAD50 and NBS1, to form MRN, which initially processes DNA DSBs before HRR or NHEJ repair pathways are activated.

ATLD shows progressive cerebellar ataxia, and progressive neurodegeneration of the cerebellum, as A-T does; however, unlike A-T, ATLD is not associated with telangiectasia, immune deficiency, and there are no reports of cancer [107]. ATLD also has a later onset than A-T and a slower progression of the disorder, which makes it a less severe condition than A-T in the early years [107]. The mutations in the MRE11 gene are hypomorphic, as knock-out mice for the MRE11 gene results in early embryonic lethality [108].

1.7.3 Nijmegen Break Syndrome

Nijmegen break syndrome (NBS) is caused by mutation of NBS1, which results in defective NBS1 protein [107, 109]. NBS1 is also part of the MRN complex but has a very different phenotype than ATLD. NBS is characterised by microcephaly, immunodeficiency, growth retardation and susceptibility to cancer [110]. There is no obvious neurodegeneration in this disorder.

NBS1 mutations interfere with the DNA repair function, by causing hypersensitivity to DSBs, which is why microcephaly is observed, due to the huge increase in neuronal cells lost during development [87]. The mutations in the NBS1 gene are hypomorphic, as germline deletion is lethal during early embryonic development [111].

1.7.4 Nijmegen Break Syndrome-Like Disorder

There has been recent evidence that two germline mutations in the RAD50 gene, gives rise to a low level of unstable RAD50, and results in a Nijmegen break syndrome-like disorder (NBSLD), which is similar to NBS except that there is no associated immunodeficiency [112].

A RAD50 deficiency results in reduction of ATM autophosphorylation, and also an impaired radiation-induced phosphorylation of the target proteins of ATM [112]. It also affects the cell-cycle checkpoint proteins present in the G1 and S phase by impairing their function [112]. RAD50 deficiency also results in a decrease in the expression levels of NBS1 and MRE11, the components that form a complex with RAD50 to form MRN [112].

1.7.5 Summary of Neurological Defects

Evidence for the neurological phenotypes that can occur due to a defective DDR resulting from mutant DNA repair proteins can be shown by the diseases/syndromes such as A-T, ATLD, NBS, NBSLD. Neurological symptoms arising from these defective repair processes highlights the

importance of a high-fidelity repair mechanism for neuronal cells, such as HRR.

As seen with many of the DNA DSB repair enzyme-related diseases discussed, ataxia is a common neurological phenotype. Purkinje cells in cerebellum are more sensitive to DNA damage than other neuronal cell types, as shown by the phenotype of ataxia, which is one of the main phenotypes that arises from mutant DNA repair proteins. A possible reason for this selective vulnerability is that Purkinje cells are large and have large nuclei due to less genome-wide condensation [113]. This chromatin state allows the cells to be exposed to more DNA damage than neurons than in a condensed chromatin structure.

1.8 Evidence for HRR in proliferating neuronal cells

Previous research performed in the Langley laboratory (unpublished) shows that HRR repair occurs in proliferating neuronal cells (Figure 1.5). For these experiments, HT22 cells were used. These cells are derived from a mouse neuronal hippocampal cell line. The HT22 cells were stably transfected with a DR-GFP transgene reporter system [114], which is engineered to contain a full-length green fluorescent protein (GFP) gene with a 5'-premature stop codon/*I-SceI* recognition sequence. *I-SceI* restriction endonuclease has no recognition sequence in the mouse genome, so in each cell the expression of *I-SceI* would induce a single DSB in the 5'-premature stop codon/*I-SceI* recognition sequence of the GFP. The reporter vector also contained a portion of the wild-type GFP sequence, which and provide a template for HRR if it were to occur after *I-SceI* expression. In this case, the GFP 5'-premature stop codon would be removed and a functional GFP protein would be detected by immunofluorescence (Figure 1.4).

The assay showed that HRR occurred in proliferating neurons (Figure 1.5). This was an experiment to validate the assay and show that neuronal cells were capable of HRR. The next step after this project is to show that HRR can occur in non-proliferating neuronal cells.

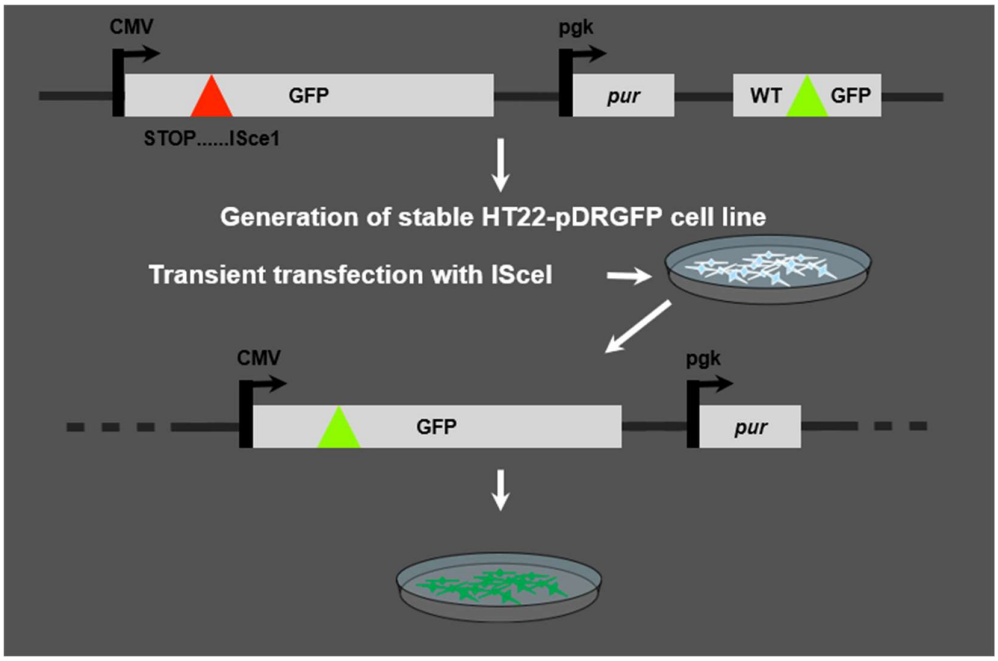

Figure 1.4 HRR assay, using a DR-GFP transgene reporter system, to determine if HRR occurs in proliferating neuronal cells. CMV is a promoter used to drive gene expression. Puromycin resistance gene *pur* is used as a selectable marker, as cells are treated with puromycin.

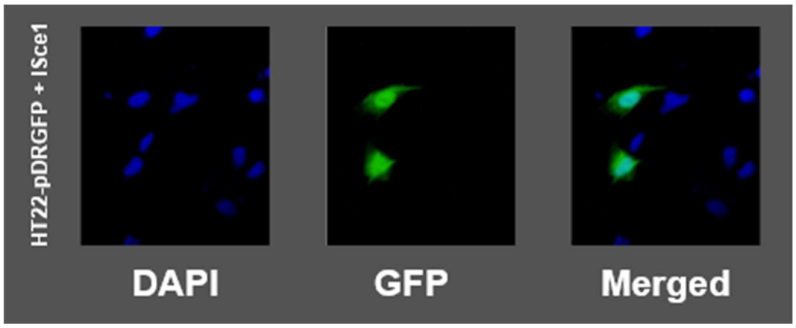

Figure 1.5 HT22-pDRGFP cells transfected with I-SceI. Blue stain = DAPI. Green stain = GFP

1.9 Project – Do Neurons Repair DNA Double-Strand Breaks by Homologous Recombination Repair?

Neurons are terminally differentiated, non-dividing cells that accumulate between 10 and 50 DNA DSBs in each cell every day [41]. This is a considerable amount of DNA damage, and if left unrepaired it can lead to the formation of DNA lesions, lost genetic information, and mutagenesis, which can contribute to neurodegenerative pathologies [42]. Because of these severe consequences, it seems that a high-fidelity process to repair these strand breaks would be crucial.

Previous research in a mouse hippocampal cell line, HT22 cells, has shown that HRR can occur in proliferating neuronal cells. However, following birth, neurons are predominantly post-mitotic, and we do not yet know if HRR can be achieved in non-proliferating neurons. This previous work was the first step in determining if neuronal cells are capable of HRR. The goal of this project is to use the DR-GFP transgene reporter system [114] (Figure 1.4) in non-proliferating neuronal cells to conclusively determine whether HRR is used as a DSB repair pathway in post-mitotic neurons.

1.10 Aims and Objectives

Research Objective 1:

Differentiation protocol

(i) Determine the best differentiation protocol for N2a cells – includes counting cells before and after treatment

a. Foetal bovine serum (FBS) concentration (10% or 1%)

b. Addition of retinoic acid (RA) or no RA

(ii) Use protocol that shows best differentiation of N2a cells (determined by cell counting) and further test its differentiation by:

a. EdU incorporation

b. Immunofluorescent microscopy

Research Objective 2:

Amplify and sequence DR-GFP transgene reporter and I-SceI expression plasmids. Establish a neuronal cell line that contains stably integrated DR-GFP in its genome

(i) Transform DH5-alpha competent *E. coli* bacterial cells with DR-GFP transgene reporter or I-SceI expression plasmids. Culture/expand transformed bacteria and purify DR-GFP or I-SceI plasmids

(ii) Confirm plasmids by restriction endonuclease digestion mapping

(iii) Transfect N2a cell line (ATCC CCL-131) with DR-GFP plasmid and select for stable genomic integration using puromycin (plasmid contains a puromycin resistance gene). This will generate a stable cell line containing DR-GFP that can be tested under different conditions for HRR

(iv) Test for integration by PCR

Research Objective 3:

Examine whether HRR occurs in proliferating neurons

(i) N2a-DRGFP cells will be tested for HRR

a. N2a-DRGFP cells will be transfected with I-SceI vector to induce DSB at the N-terminal *I-SceI* restriction endonuclease/stop site of DR-GFP

b. GFP-immunofluorescence microscopy will be used to monitor neuronal DNA repair: If repair of this site occurs through NHEJ no fluorescence will be observed; if repair of this site occurs through HRR fluorescence will be observed

Research Objective 4:

Examine whether HRR occurs in post-mitotic neurons

(i) N2a-DRGFP cell line will be differentiated using 10μM retinoic acid / 1% FBS. This will generate post-mitotic neurons (which can be demonstrated by EdU incorporation and immunofluorescence using DNA staining)

(ii) Post-mitotic N2a neurons will be transfected with I-SceI vector to induce DSB at the N-terminal *I-SceI* restriction endonuclease/stop site of DR-GFP

(iii) GFP-immunofluorescence microscopy will be used to monitor neuronal DNA repair: If repair of this site occurs through NHEJ no fluorescence will be observed; if repair of this site occurs through HRR fluorescence will be observed

Chapter 2

Materials and Methods

All methods were carried out at the University of Waikato, in either the E3.11, E3.13 (PC2 lab), or C.2.09. All experiments were carried out aseptically in areas cleaned with 70% ethanol.

This chapter contains the methods that were repeatedly performed throughout this project. Individual experimental details are written in the methods section of each chapter.

2.1 Common Solution Preparations

Solutions	Composition
N2a growth media	89% DMEM media 10% FBS 1% Penicillin-Streptomycin
1% FBS media	10% N2a growth media 90% DMEM
Retinoic acid stock solution (12.45 mM)	50 mg Retinoic acid 1.5 ml DMSO
TE (Tris-EDTA) buffer (10 µM)	5 ml 1M Tris pH 8 1 ml 0.5M EDTA pH 8 496 ml dH_2O
TAE buffer 50x stock	100 ml 0.5M EDTA pH 8 242 g Tris base 57.1 ml acetic acid dH_2O to final 1 L volume
Puromycin stock solution (50 mg/ml)	50 mg Puromycin 1 ml dH_2O

Table 2.1 Common Preparation Solutions

2.2 N2a Cells

The N2a cells have an authority number of GMC001340. The cell line used is derived from *Mus musculus*. Transformations will take place in *E. coli* cells. The bacterial transformation and mammalian transfections of these cells have the HSNO number GMD101146 and will be developed under the Facility 759's EPA approval APP201152_s67.

The N2a cell line was obtained from the -80°C cell culture inventory in the C-Block laboratories of the School of Science at the University of Waikato. The growth media for these cells was; DMEM media (Gibco) with 10% FBS (Gibco) and 1% Penicillin-Streptomycin (Thermo Fisher). The cells were kept in the incubator in C2.09 during the cell culturing process with the standard conditions: 37°C, and 5% CO_2, in a humidified incubator. The cells were passaged when they reached 80% confluency and were topped up with fresh media every other day to maintain their health and optimal growth. The cells were then moved to E3.13 (PC2 lab) once transfections began and stored in the same incubator conditions.

2.2.1 Frozen N2a Cells

Before starting experiments N2a cells were thawed. Thawing of frozen N2a cells was done rapidly to minimise cell death. To maintain the highest number of cell survival, a vial of N2a cells was thawed for 2 minutes in a 37°C water bath. Once the cells were thawed, they were centrifuged for 7 minutes at 125 x g to form a pellet. The supernatant was removed, and the pellet was resuspended in growth media. The cells were then grown in a 10 cm plate before being transferred to a 75 cm^3 flask once cells had become 80% confluent.

2.2.2 Subculture of Cells

Phosphate buffered saline (PBS) (Gibco) and growth media were warmed to 37°C in the incubator before cells were sub-cultured, to avoid cold shock to the cell when these reagents were added.

N2a is an adherent cell type. To passage the cells, media was removed, and the cells were washed briefly with 10 ml of PBS. Once PBS was removed, 1 ml of 0.25% Trypsin-EDTA (Gibco) was added. Trypsin breaks the bonds in proteins, which allowed for the cells to be dissociated from the surface of the flask. The flask was then placed in the incubator for five minutes or until it was observed under the microscope that the cells had dissociated from the surface of the flask and were in the trypsin solution. To inactivate trypsin activity, 20 ml of media was added for a 1:2 passage (10 ml for each new flask) – adjust accordingly for a larger/smaller passage. 10 ml of the media was removed and added to a new flask.

Transfection of cells occurred between passages 5 and 25 post-thaw.

2.3 LB Agar + Ampicillin Plates

Seven grams of LB Broth with agar (Lennox) (Sigma) was added to 200 ml dH_2O and mixed. The bottle was autoclaved for 20 minutes at 120°C. The LB agar mixture was then removed from the autoclave and left to cool to approximately 60°C.

A Bunsen burner was used to maintain a sterile working area and for flame sterilisation. 200 µl of 100 mg/ml ampicillin (Sigma) was added to the LB agar and mixed. Approximately 10 ml of the LB agar and ampicillin mixture was added to each petri dish. The petri dishes were left to cool for one hour, then stacked on top of each other and placed in the fridge (4°C) upside down overnight.

2.4 LB Growth Media

LB growth media was prepared by adding 6.25 g of LB Broth powder (Sigma) to 250 ml of dH_2O and mixing vigorously. The bottle was autoclaved for 20 minutes at 120°C. LB broth was then removed from the autoclave with heat resistant gloves and left to cool. LB broth was stored in the fridge (4°C) when not in use.

2.5 Agarose Gel

Agarose gels (1 to 2%) were made by mixing 1 to 2 g of UltraPure agarose powder (Invitrogen) into 100 ml of 1 x TAE buffer (Thermo Fisher) and microwaved, mixing every 30 seconds, until all agarose particles were dissolved. 2 µl of 10 mg/ml ethidium bromide was then added to the gel and mixed. This was then poured into a 15-well gel mould and left to set at room temperature. Prior to use it was submerged in 1 x TAE buffer in a DNA electrophoresis chamber.

Chapter 3

Differentiation of N2a Cell Line

3.1 Introduction

In proliferating cells, DSBs are said to occur by HRR, a high-fidelity process, as clonal expansion of misrepaired DNA could potentially lead to cancer. DSBs in post-mitotic cells, by contrast, are thought to be repaired by NHEJ, a low fidelity process, as it is less time- and energy-efficient, and because the consequences of misrepaired DNA are not as detrimental to the organism.

For this project we are investigating what DSB repair pathway is used in post-mitotic neuronal cells. Neuroblastoma cells, such as N2a, are cancer cells, which means that they are proliferative. However, given the right cell culture conditions, N2a cells can be induced towards a post-mitotic, differentiated phenotype [115]. The aim is to utilise this important feature of N2a cells to best replicate a post-mitotic neuronal state that exists *in vivo.*

The first task of this project was to determine the best post-mitotic cell induction method for N2a cells. In the first experiment, serum deprivation was used, and it was found that cells were still able to proliferate at 1% FBS concentration. We then tested 1% FBS concentration with retinoic acid (RA), which showed non-proliferative state as shown by cell counting. Once the optimal FBS and retinoic acid (RA) concentration was found by cell counting, an EdU incorporation assay was used to definitively conclude that the N2a cells were not proliferating.

3.2 Methods

3.2.1 Induction of a Non-Proliferative N2a Cell State

N2a cells need to be post-mitotic for the HRR experiment. Different differentiation media compositions were investigated to determine which cell culture conditions would best promote a non-proliferative state in the N2a cells. To test different cell culture methods, 24-well plates were used.

3.2.1.1 Serum Deprivation

The first culture conditions that were piloted were DMEM with 10% serum versus DMEM with 1% serum. Cells were placed into 24-well plates at a density of 1 x 10^4 cells per well. Cells were first cultured in 0.5 ml of growth media per well and placed in the incubator for 24 hours so the cells could adhere to the plate and recover.

After 24 hours, one well was trypsinised and the cells were counted by haemocytometer [116], to determine a starting cell number (10% FBS condition). The media was changed in each remaining well, with one of the two conditions; 10% FBS or 1% FBS.

Cells were counted daily for 7 days per condition to establish a growth curve. This experiment was carried out in duplicate and results were averaged.

3.2.1.2 Retinoic Acid Addition and Serum Deprivation

The second cell culture conditions to be piloted were to employ a range of retinoic acid (RA) concentrations in addition to the serum deprivation (1% FBS media). Different concentrations of RA used were; 5 μM, and 10 μM.

Cells were first seeded in 24-well plates at a density of 1 x 10^4 cells with 0.5 ml of growth media. After 24 hours the media was changed to one of the conditions as stated in Figure 3.1. 10% FBS and 1% FBS conditions were used as control groups.

Cells were cultured and observed for toxicity for 7 days. The media in the 24-well plates was changed every 3 days so that the nutrients for the cell's growth was not exhausted. Each day one well for each condition was trypsinised and counted by haemocytometer. The standard growth curve was calculated, and conditions were plotted against this to determine cell differentiation. This experiment was carried out in duplicate and results were averaged.

10% FBS	1	2	3	4	5	6
1% FBS	7	8	9	10	11	12
1% FBS, 5 µM RA	13	14	15	16	17	18
1% FBS, 10 µM RA	19	20	21	22	23	24

Figure 3.1 Conditions for 24-well plate differentiation experiment

3.2.1.3 EdU Incorporation

The EdU incorporation assay was achieved by the use of a Click-iT EdU Imaging Kit (Thermo Fisher) and is an adaption of the more traditional BrdU cell proliferation assay. EdU (5-ethynyl-2'-deoxyuridine) is a nucleoside analog of thymidine and is incorporated into DNA during DNA synthesis. EdU detection is based on click chemistry, which is a reaction between a picolyl azide and an alkyne. The EdU contains the alkyne and the Alexa Fluor dye contains the picolyl azide. The picolyl azide-Alexa Fluor dye is small in size, so it can readily gain access to the DNA using mild detergent permeabilization to detect the incorporation of EdU. An Alexa Fluor 594 (red)

dye was used so as to be compatible with GFP (green) and DAPI (blue) fluorescence in later experiments. As EdU will only be incorporated into DNA if the cell is proliferating, a lack of red fluorescence would be indicative of non-proliferating cells.

Cells were seeded in 24-well plates at a density of 1 x 10^4 cells with 0.5 ml of growth media. After 24 hours the media was changed to one of the conditions: 10% FBS, 1% FBS, or 1% FBS containing 5 µM or 10 µM RA, as described in Figure 3.1.

After 7 days of culture, cells were removed from the incubator. The media was removed from cells and the cells were washed with PBS. This was done to remove any cell debris and residual media. The PBS was removed and 1.5 ml of each culture media containing 10 µM EdU was added to each well. Cells were then incubated for 36 hours to allow time for the EdU to incorporate into DNA if the cells were proliferative.

After 36 hours, the media was removed from the cells and cells were washed with PBS. 1 ml of 3.7% formaldehyde in PBS was added to each well and incubated for 15 minutes. Formaldehyde is a cross-linking agent that fixes cells and preserves their cellular morphology. After 15 minutes, the formaldehyde was removed, and the cells were washed twice with 1 ml of 3% BSA in PBS. When the wash solution was removed, 1 ml of 0.5% Triton X-100 (Sigma Aldrich) in PBS, was added to each well and incubated at room temperature for 20 minutes. Triton X-100 was added as it permeabilises the cell membrane.

A reaction cocktail was made containing 1X Click-iT reaction buffer (5.16 ml), CuSO4 (240 µl), Alexa Fluor azide (14.4 µl), and reaction buffer additive (6 ml). Triton X-100 was removed from the cells, and cells were washed twice with 3% BSA in PBS. The wash solution was removed and 500 µl of the reaction cocktail was added to 12 of the 24 wells (Row 2, 3, and 4 were used; Figure 3.1). The 24-well plate was gently rocked to evenly distribute the reaction cocktail. The plate was covered in tinfoil to protect it from light

and was left to incubate at room temperature for 30 minutes. The reaction cocktail was then removed, and the cells were washed with 1 ml of 3% BSA in PBS.

The wash solution was removed, and the cells were washed again, with 1 ml PBS. The wash solution was removed and 1 ml of DAPI (5 μg/ml) in PBS was added to the wells. DAPI is a blue stain that can stain living and permeabilised cells. The plate was covered in tinfoil to protect it from light and the plate was left to incubate at room temperature for 30 minutes. The DAPI solution was then removed and the cells were washed twice with 1 ml of PBS. The PBS was then removed.

The cells were then taken to the confocal room to be imaged.

3.2.1.3.1 Confocal Microscopy

Two laser channels were used;

Channel 1 settings:

Dye – Alexa Fluor 594

Excitation wavelength – 590 nm

Emission wavelength – 615 nm

Channel 2 settings:

Dye – DAPI

Excitation wavelength – 358 nm

Emission wavelength – 461 nm

Once cells had been visualised photos were taken and cells were counted. Three photos were taken for each condition. Blue cells with red stain and blue cells without red stain were counted separately. Cells that were stained red but were not stained blue were not included.

3.3 Results

3.3.1 Growth Curve of N2a cells

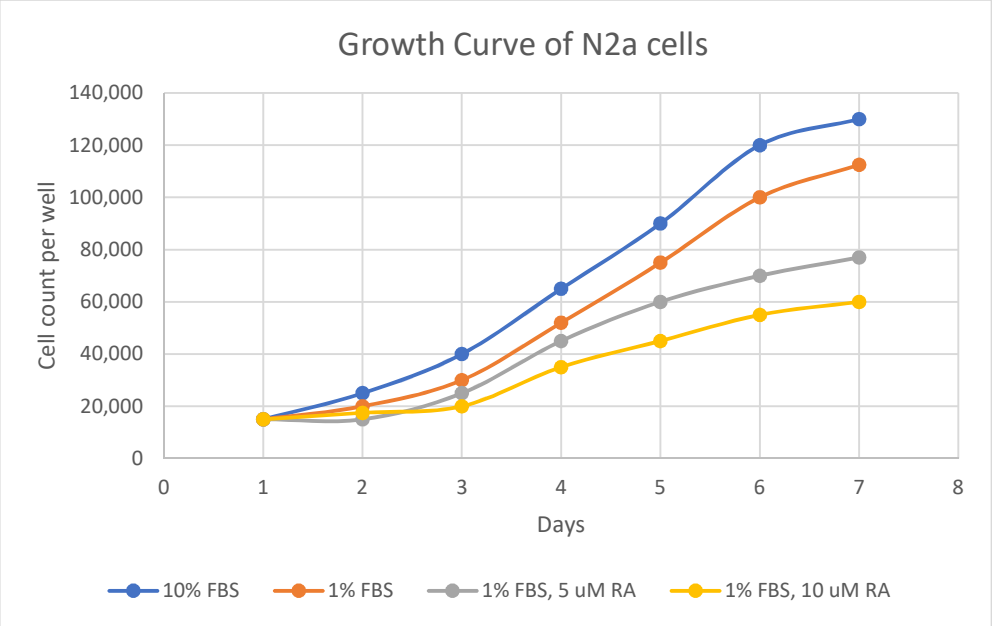

Figure 3.2 Growth curve of N2a cells with differentiation media

From the growth curve (Figure 3.2), all cells observe a lag phase for approximately the first three days followed by an exponential growth phase. After 6 days the rate of division for cells begins to decline, which is most likely due to the high level of confluency and cell contact inhibition.

Cells in the 10% FBS condition grow the most rapidly, as to be expected as this is the optimal growth medium for N2a cells. Cells are still able to grow and divide rapidly in the serum deprivation condition of 1% FBS. The addition of RA shows to have slowed cell growth and division, as can be seen in the 1% FBS + 5 μM RA, and 1% FBS + 10 μM RA conditions, with the 10 μM RA condition showing the least cell growth. This data suggests that RA in addition to serum deprivation results in decreased cell growth.

3.3.2 EdU Incorporation

10% FBS Condition		
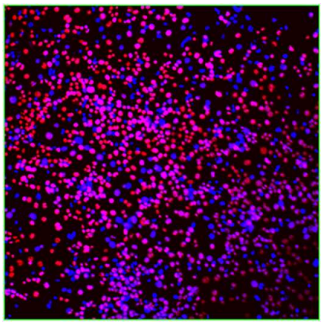 A	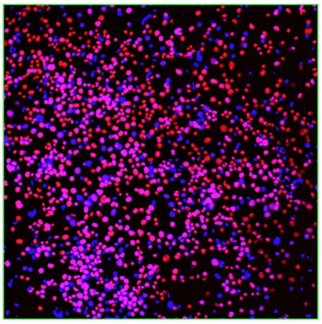 B	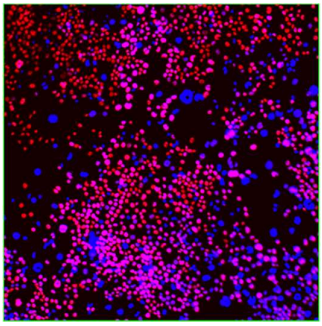 C
1% FBS Condition		
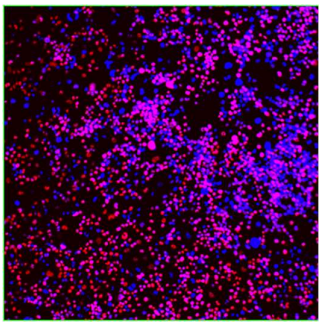 A	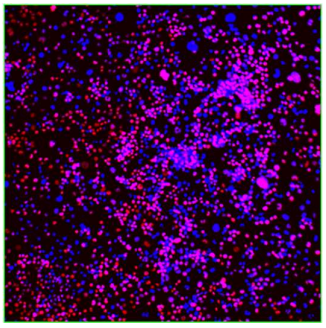 B	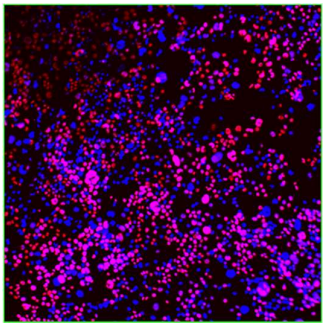 C
1% FBS + 5 μM RA Condition		
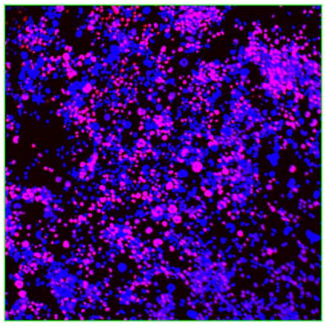 A	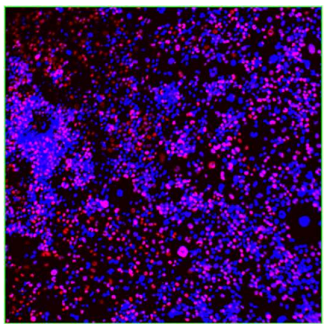 B	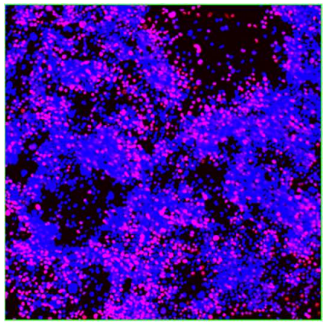 C

1% FBS + 10 µM RA Condition		
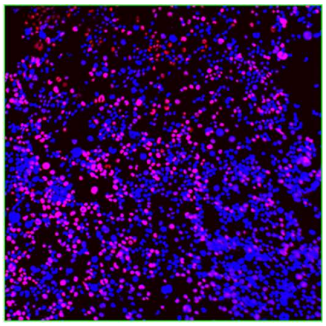 A	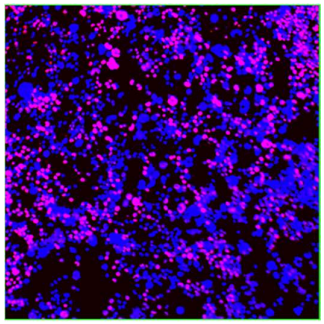 B	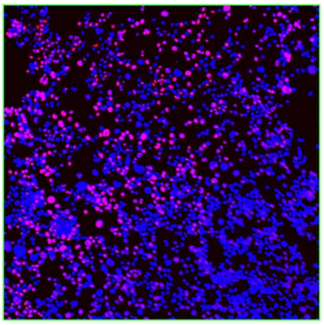 C

Table 3.1 EdU incorporation assay in 10x magnification for 10% FBS Condition, 1% FBS Condition, 1% FBS + 5 µM RA Condition, and 1% FBS + 10 µM RA Condition. Blue cells = cells that have not incorporated Edu into its DNA; Red cells = cells that have incorporated EdU into its DNA.

The incorporation of EdU into each cell condition can be seen in Table 3.1. DAPI is a blue fluorescent DNA stain and can visualise nuclear DNA in living and fixed cells. This means that all cells will be stained blue. EdU is a red fluorescent marker that is incorporated into proliferating DNA, so will only stain proliferating cells and not cells that are non-dividing. Cells that have a blue and red fluorescence show that the cells are alive and are proliferative. Cells that are only stained blue and not red show cells that are not proliferative.

The 10% FBS condition has the greatest number of red and blue co-staining, followed by the 1% FBS condition. The addition of RA as seen in the 1% FBS + 5 µM RA and 1% FBS + 10 µM RA conditions, shows less red and blue co-stained cells than the 10% FBS and 1% FBS conditions. These results were quantified by cell counting.

10% FBS Condition	1% FBS Condition
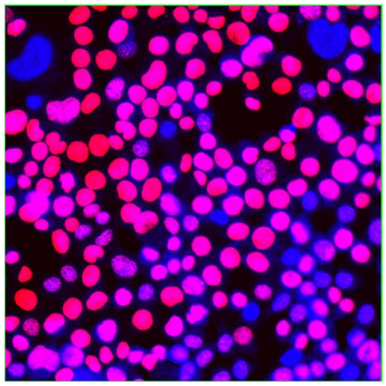	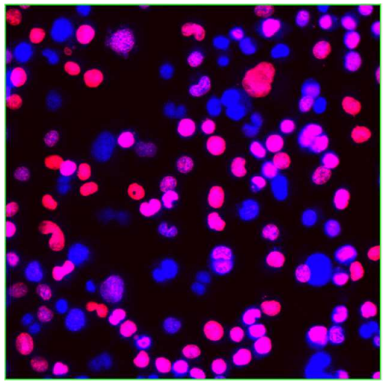
1% FBS, 5 µM RA Condition	**1% FBS, 10 µM RA Condition**
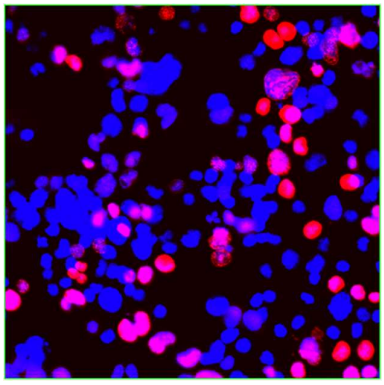	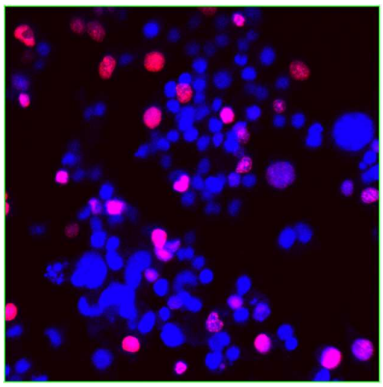

Table 3.2 EdU incorporation assay at 40x magnification for 10% FBS Condition, 1% FBS Condition, 1% FBS, 5 µM RA Condition, and 1% FBS, 10 µM RA Condition. Blue cells = cells that have not incorporated Edu into its DNA; Red cells = cells that have incorporated EdU into its DNA.

40x magnification images of the EdU incorporation assay (Table 3.2) were taken to represent the differences in the number of proliferative vs non-proliferative cells. In the 10% and 1% FBS conditions it is clear that there is more proliferating cells than non-proliferating cells. In the conditions with the addition of RA it is clear than there are more non-proliferating cells vs proliferating cells.

3.3.2.1 Cell Count

Cells from each image in Table 3.1 were counted and their results were tallied into Tables 3.3 – 3.6. This showed the number of proliferative cells vs non-proliferative cells and showed the best differentiation method for N2a cells.

10% FBS Condition					
	Red cells	Blue cells	Total cells	Proliferating cells	Non-proliferating cells
A	1037	337	1374	75%	25%
B	1011	259	1270	80%	20%
C	1030	266	1296	79%	21%
			Average	**78%**	**22%**
			Standard Deviation		**2.16**

Table 3.3 Cell count for 10% FBS condition after EdU incorporation.

Table 3.3 shows that in the 10% FBS condition 78% of cells are proliferative, and only 22% of cells are non-proliferative. Because this condition is the growth media for N2a cells, this result shows that cells are able to grow and divide.

1% FBS Condition					
	Red cells	Blue cells	Total cells	Proliferating cells	Non-proliferating cells
A	1143	373	1516	75%	25%
B	715	418	1133	63%	37%
C	1075	511	1586	67%	33%
			Average	**68%**	**32%**
			Standard Deviation		**4.99**

Table 3.4 Cell count for 1% FBS condition after EdU incorporation.

Table 3.4 shows that in the 1% FBS condition 68% of cells are proliferative, and only 32% of cells are non-proliferative. This result shows that serum deprivation alone is not enough to differentiate N2a cells as the cells are still highly proliferative in the 1% FBS condition.

1% FBS, 5 µM RA Condition					
	Red cells	Blue cells	Total cells	Proliferating cells	Non-proliferating cells
A	735	901	1636	45%	55%
B	954	1005	1959	49%	51%
C	1622	2419	4014	40%	60%
			Average	**45%**	**55%**
			Standard Deviation		**3.68**

Table 3.5 Cell count for 1% FBS, 5 µM RA condition after EdU incorporation.

Table 3.5 shows that in the 1% FBS condition with the addition of 5 µM RA, 45% of cells are proliferative and 55% of cells are non-proliferative. This result shows that serum deprivation with the addition of RA shows a higher percent of cell differentiation than serum deprivation alone, as more than half of the cells have differentiated after 7 days, whereas in the 1% FBS condition only one-third of cells had differentiated. However, there is still a significant number of cells that are able to proliferate, so a higher concentration of RA seems likely to best differentiate N2a cells.

1% FBS, 10 µM RA Condition					
	Red cells	Blue cells	Total cells	Proliferating cells	Non-proliferating cells
A	367	1003	1370	27%	73%
B	552	942	1494	37%	63%
C	585	1126	1711	34%	66%
			Average	**33%**	**67%**
			Standard Deviation		**4.19**

Table 3.6 Cell count for 1% FBS, 10 µM RA condition after EdU incorporation.

Table 3.6 shows that in the 1% FBS condition with the addition of 10 μM of RA, 33% of cells are proliferative and 67% of cells are non-proliferative. This result shows that two-thirds of all cells are non-dividing, which is significantly higher than serum deprivation alone (only one-third of cells non-dividing) and has more non-dividing cells than the addition of 5 μM RA (roughly half the cells were non-dividing). Higher concentrations of RA were used in preliminary studies (data not shown) and was shown to be toxic, as there was a loss of cells. The best differentiation method for N2a cells, as shown by EdU incorporation and cell counting is 1% FBS with the addition of 10 μM RA, over a period of seven days.

3.3.2.2 T-Test

10% FBS	1% FBS	1% FBS, 5 μM RA	1% FBS, 5 uM RA
25%	25%	55%	73%
20%	37%	51%	63%
21%	33%	60%	66%
P-value	**0.195375**	**0.007221025**	**0.001025669**

Table 3.7 T-Test of 10% FBS and 1% FBS; 1% FBS, 5 μM RA; and 1% FBS, 10 μM RA.

A t-test was performed to determine the statistical significance between the growth condition (10% FBS) and the differentiation conditions (1% FBS; 1% FBS + 5 μM RA; and 1% FBS + 10 μM RA) (Table 3.7). At the α=0.05 level there is sufficient evidence to conclude that there is a significant difference between the growth condition and the 1% FBS, 5 μM RA (p=0.0072) and 1% FBS, 10 μM RA (p=0.0010). However, at the α=0.05 level there is not sufficient evidence to conclude that there is a significant difference between the growth condition and the 1% FBS condition (p=0.19).

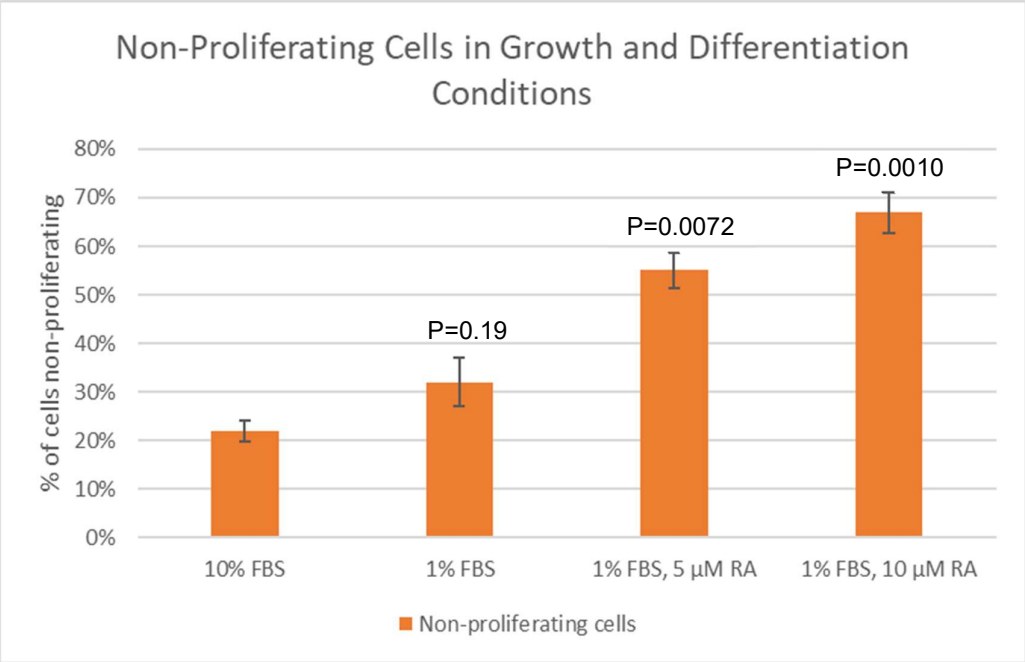

Figure 3.3 The percentage of non-proliferating cells in growth and differentiation conditions, with error bars and p-values.

Figure 3.3 summarises the percentage of cells that are non-proliferative in each growth and differentiation condition. This graph shows that serum deprivation and RA addition results in a higher percentage of non-proliferative cells and this is statistically significant. 1% FBS and 10 µM RA also has higher percentage of non-proliferative cells than 1% FBS and 5 µM of RA which is statistically significant.

The results from cell counting showed that even after 7 days in differentiation media the 1% FBS and 10 µM RA condition still had proliferative cells. This could have been due to the cell lineage fate of these cells. Some of the cells may have differentiated into glial cells, which can maintain the ability to divide.

3.4 Discussion

The objective of this chapter was to determine the optimal differentiation method for N2a cells. A standard growth curve of N2a cells in growth media

under normal incubator conditions was generated. Serum deprivation was initially used to differentiate N2a cells; however, it was found through cell counting that cells were still highly proliferative. Because of this, serum deprivation with the addition of RA was used. Cells were counted over the span of seven days and these results were plotted against the standard growth curve of N2a cells in growth media. The growth curve of these cells under different conditions showed that 1% FBS, and 10 μM RA over the course of seven days showed the lowest proliferation.

After cell counting, an EdU incorporation assay was used to show the number of non-proliferative cells for each condition and definitively conclude if cells were not proliferating. EdU incorporation showed that the 1% FBS + 10 μM RA condition had the highest number of cells that were non-proliferating (67%). From this, it was established that for N2a cells the optimal protocol for differentiation was to treat cells with 1% FBS media and 10 μM RA over the course of seven days. This differentiation protocol will be used in the HRR experiment to test if HRR occurs in non-proliferating neuronal cells.

This chapter was important for learning the protocol for EdU staining. The aim of this project is to investigate whether HRR occurs in non-proliferative neuronal cells. Thus, in the HRR experiment, cells can be differentiated using 1% FBS and 10 μM RA media, as this was found to be most effective, and will be stained with EdU and DAPI so only cells that are non-proliferative, will be included. In the HRR experiment, if a cell shows green fluorescence and blue fluorescence, and no red fluorescence, it will confirm that HRR has occurred in post-mitotic neuronal cell. From this chapter, it was confirmed that EdU is a suitable test to show proliferative vs non-proliferative cells.

A growth curve shows the phases in which a cell culture generally goes through. The first phase is the growth phase where the culture have a delayed growth due to the stress of sub-culturing and the small number of cells. The cells then go into an exponential or log phase, where the cells are growing optimally and dividing rapidly. After this phase, cells enter a

stationary phase in which the cells growth reaches a plateau, usually due to the exhaustion of media or cell contact-inhibition because of confluency. In our experiment, the media was changed in the cells every three days to prevent the depletion of nutrients and allow the cells to grow – unless the media conditions caused the differentiation of the cells, which would be seen by a decrease in cell growth.

In initial experiments for cell counting, cells were seeded at two different densities: 1 x 10^4 cells per well and 2 x 10^4 cells per well. It was found that cells seeded at 2 x 10^4 became overcrowded quickly and needed to be sub-cultured, whereas cells seeded at 1 x10^4 cells per well did not need to be sub-cultured. Because of this, in all future experiments the cells were seeded at the density of 1 x 10^4 cells. One problem that was encountered with this density was that the 10% FBS condition cells became fully confluent after seven days. Because of this, all cells were washed twice with PBS before the EdU assay to ensure that dead or unhealthy cells were removed and allowed the other cells to remain healthy.

Various studies have used RA and serum deprivation to differentiate cells [117-119]**.** However, different concentrations are used, requiring the need for multiple media compositions to be tested. Before the 5 μM and 10 μM concentrations were chosen, a preliminary experiment was performed in a 6-well plate with RA concentrations of 5 μM, 10 μM, 20 μM, and 50 μM. It was found that 20 μM and 50 μM RA were toxic to the N2a cells and resulted in a large number of cell death, which is why 5 μM and 10 μM concentrations were used.

EdU incorporation is a cell proliferation assay that is an alternative to a BrdU assay. BrdU is a nucleoside that is an analog of thymidine. BrdU incorporation is an antibody-based reaction and requires denaturation of DNA to detect the incorporated nucleoside. BrdU is a time-consuming process and is less accurate than EdU, as artifacts may arise from the denaturation and antibody steps. EdU incorporation was a simple and easy assay to confirm the proliferative state of cells.

Chapter 4

DNA Vectors and Generation of a Stable Cell Line

4.1 Introduction

To test if HRR can occur in post-mitotic neurons, DNA plasmids DR-GFP and I-SceI needed to be amplified and purified. Once purified, DR-GFP can be transfected into N2a cells and create generate a stable cell line of N2a-DRGFP cells.

The process of amplifying and purifying DNA plasmids involves bacterial transformation. This process utilises the concept of horizontal gene transfer. This is the process of genetic material being passed between bacteria by means other than from parent to offspring (vertical gene transfer) and is very rare in nature. Because of this, specialised cells that have a cell membrane more permeable have been engineered, which allows genetic material to enter the cell after heat shock. After the plasmid DNA has been transformed into the bacterial cell, the DNA can be purified by miniprep.

The transfection of the purified DR-GFP plasmid into proliferating N2a cells is achieved by lipofection. Lipofection allows negatively charged DNA to aggregate with positively charged liposomes. Liposomes are a vesicle that can easily pass through the cell membrane, thus allowing the DNA to enter the cell. Once cells have been transfected with DR-GFP, puromycin is added to media as DR-GFP has a puromycin resistance gene. After treatment with puromycin only cells that have stable integration of DR-GFP in their genome will survive and will generate a stable cell line of N2a-DRGFP cells.

4.2 Methods

4.2.1 Bacterial Transformation

Competent *E.coli* cells, which have an altered cell wall that is designed to make cells more permeable and allow genetic material to enter the cell, are used for the process of bacterial transformation.

One tube (500µl) of DH5α competent *E. coli* (Invitrogen) was removed from the -80°C freezer and immediately placed on ice. They were left to sit on the ice for 15 minutes to slowly thaw.

Two plasmids stored on filter paper – I-SceI and DR-GFP – were added to labelled Eppendorf tubes. These two plasmids were sourced from Weil Cornell Medical College in New York. TE buffer (60 µl) was added to each tube, vortexed, then centrifuged at 16,100 rpm for 30 seconds.

Another three Eppendorf tubes were labelled with the following: I-SceI, DR-GFP, and Control. Competent cells (110 µl) were added into each of the samples and 5 µl of plasmid was added to the correct tube (5 µl of dH2O added to control). The samples were incubated on ice for 30 minutes. The samples were then heat shocked in the thermomixer, which was set to 42°C for 30 seconds. They were removed from the thermomixer and placed directly onto ice and cooled for 2 minutes. LB growth media (950 µl) was added to each tube and placed in the shaking thermomixer, at 37°C, for an hour. The samples were then centrifuged for 30 seconds at 13,000 rpm to form a pellet. The media was removed so that only the pellet remained, and it was resuspended in 200 µl of LB growth media.

Four LB agar plates were removed from the fridge and kept close to the flame of a Bunsen burner, to keep the area sterile. After this, 100 µl of each sample was spread onto separate LB agar plates. LB agar plates were incubated in a 37°C incubator overnight. Overnight the LB agar plates formed colonies, except the control sample that did not contain any DNA.

Once removed from the incubator they were stored in the fridge until ready to use.

Culture tubes (4 each for DR-GFP and I-SceI) were placed next to the flame of a Bunsen burner. 3 ml of LB growth media was added to each tube. The LB agar plates were removed from the fridge and placed close to the flame. A sterile pipette tip was used to remove a single colony from the DR-GFP LB agar plate. Once a colony had been removed, the pipette tip was placed in a DR-GFP labelled culture tube. This was repeated three more times until there was a single colony in each DR-GFP culture tubes. The same process was repeated for the I-SceI LB agar plate and culture tubes. The culture tubes were incubated in the shaking incubator overnight. 1.5 ml of the overnight cultures were added to labelled 1.6 ml Eppendorf tubes and centrifuged at 8000 rpm for 2 minutes to form a pellet. The remaining culture/tubes were stored in fridge until needed.

4.2.2 Mini Prep

Mini prep is the process of isolating plasmid DNA from bacteria and was achieved by the use of a GeneJET plasmid miniprep kit (Thermo Fisher). The solutions were made up to their specifications.

Supernatants were removed from pelleted cultures and the pellets were resuspended in 250 µl of resuspension solution. The tubes were vortexed to ensure no clumps remained in the solution. 250 µl of the lysis solution was added to each tube and was mixed by inversion 4-5 times. Next, 350 µl of the neutralisation solution was added to each tube and mixed by inversion.

Lysates were centrifuged for 5 minutes at 12,000 x g so that the cell debris and chromosomal DNA would form a pellet. The supernatant from each lysate was then transferred into labelled GeneJET spin columns and centrifuged for 1 minute at 12,000 x g. The flow-through was discarded and the column placed back on the same collection tube.

The GeneJET spin columns were washed by the addition of 500 µl of wash solution and then centrifuged at 12,000 x g for 1 minute. The flow-through was then discarded and the column placed back on the same collection tube. This wash step was repeated again, and the spin column was centrifuged at 12,000 x g for a further minute to ensure that all residual wash solution was removed.

The GeneJET columns were then transferred into labelled 1.5 ml Eppendorf tubes and 50 µl of the elution buffer was added into the spin column. These were then incubated at room temperature for 2 minutes before they were centrifuged at 12,000 x g for 2 minutes. The columns were then discarded, and the tubes were stored at -20°C.

4.2.3 Nanodrop Readings

After DNA plasmids had been purified, 2µl of the sample was tested on the Nanodrop2000 (Thermo Fisher) machine to determine the quantity and quality of the DNA. Absorbance at 280nm is used as an indicator of the purity of nucleic acid samples. A 260/280 ratio of ~ 1.8 is accepted as pure for DNA.

4.2.4 Restriction Digest of Plasmid DNA

Reagents	**Single Restriction Digest**	**Master Mix**
DNA	2 µl	-
10x Buffer (Thermo Fisher)	2 µl	17 µl
Enzyme (*HindIII*)	0.95 µl	8 µl
dH2O	15.05 µl	128 µl
Total	20 µl	153 µl

Table 4.1 Restriction endonuclease digestion components.

Restriction endonucleases are able to cut DNA at specific recognition sites into smaller fragments. HindIII (Thermo Fisher) is a restriction endonuclease that is able to cut both I-SceI and DR-GFP DNA plasmids at known sites. With this information it is possible to restriction map the plasmids and determine if the plasmid isolated is correct by running the cleaved DNA on an agarose gel.

Restriction digestions were carried out on eight plasmids – four for I-SceI and four for DR-GFP. DR-GFP sample tubes were labelled 1-4, while I-SceI sample tubes were labelled 5-8. A master mix was made in a 1.5 ml Eppendorf tube with the components stated in Table 4.1 and then aliquoted into the sample tubes as per the single restriction digest in Table 4.1. DNA was not added into the master mix as it was added once the mix had been aliquoted into labelled tubes.

The Eppendorf tubes containing the purified plasmids were removed from the -20°C freezer. DR-GFP plasmids 1-4 were added to the restriction digestion tubes labelled 1-4 (2 µl per tube). I-SceI plasmids 1-4 were added to the restriction digest tubes labelled 5-8 (2 µl per tube). The tubes were then incubated for 2 hours at 37°C.

4.2.4.1 Agarose Gel Electrophoresis

A 1% agarose gel was made to specifications in Chapter 2.5. Gel loading buffer was added to each sample of I-SceI and DR-GFP. A 1 kb ladder was added to the first and last lane. DR-GFP and I-SceI samples were then added to the lanes. The gel was run at 60 V for approximately 1.5 hours – the dye was observed 75% down the gel. The gel was removed and taken for imaging.

Gels were imaged by ethidium bromide fluorescence using a UV gel documentation system (Image Quant LAS 400). *HindIII* cuts DR-GFP to produce fragments of the following sizes: 5542 bp, 2298 bp, and 806 bp. *HindIII* cuts I-SceI to produce fragments of the following sizes: 4717 bp and

948 bp. These DNA fragments can be separated and visualised a DNA gel and determine if the plasmids are correct.

4.2.5 Transfection of N2a cells with DR-GFP

N2a cells were transfected with DR-GFP by the process of lipofection. DNA is negatively charged, and it can aggregate with positively charged liposomes. Liposomes are a vesicle that can easily pass through the cell membrane, thus allowing the DNA to enter the cell.

N2a cells were plated on 3 x 10 cm plates at a confluency of approximately 60%. They were left in the incubator for 24 hours to recover and grow. The next day, cells had reached 80% confluency and were ready to transfect.

Components	**Lipofectamine Tube (x2)**	**DR-GFP 1 Tube**	**DR-GFP 2 Tube**
Lipofectamine (Thermo Fisher)	40 µl	-	-
DNA	-	31.8 µl	41.2 µl
Serum-free media	560 µl	568.2 µl	558.8 µl

Table 4.2 Components used for transfection of DR-GFP into N2a cells

DR-GFP 1 and DR-GFP 2 were removed from the -20°C freezer. DR-GFP samples were diluted to a concentration 14 µg/ml of DNA by dilution with serum-free media.

Components from Table 4.2. were made to specifications. Two lipofectamine samples were made, with lipofectamine added to the media slowly and mixed to prevent aggregates from being formed. The DR-GFP 1 sample was added slowly to a lipofectamine sample and mixed thoroughly. This was repeated for the DR-GFP 2 sample and other lipofectamine

sample. These were incubated at room temperature for 5 minutes. After incubation, 6.8 ml of media was then added to each sample.

N2a cells on 3 x 10cm plates were removed from the incubator and their media was removed. They were washed briefly with 5 ml PBS. DNA/lipofectamine/media complexes were then added to 10 cm plates. The final plate was a control, where 8 ml of serum-free media was added to the plate. N2a plates were then placed back in the incubator for 4 hours. After 4 hours, the media was replaced with 10 ml of a growth media.

4.2.6 Puromycin Selection

Transfected N2a cells were treated with puromycin in growth media the next day. DR-GFP has a puromycin resistant gene, so only transfected cells survive. Puromycin was added to media at a concentration of 2 μg/ml for two weeks and one week at 3 μg/ml, to ensure that all cells contained the DR-GFP plasmid in their genome. Cells were passaged every three days.

4.3 Results

4.3.1 Nanodrop Readings

Sample	DNA concentration (ng/μl)	260/280
I-SceI.1	223.0	1.87
I-SceI.2	281.5	1.88
I-SceI.3	337.4	1.89
I-SceI.4	388.9	1.82
DR-GFP.1	440.4	1.88
DR-GFP.2	339.5	1.89
DR-GFP.3	93.0	1.89
DR-GFP.4	449.3	1.88
pEGFP	211.0	1.88

Table 4.3 Nanodrop Readings of I-SceI, DR-GFP and pEGFP.

The nanodrop readings show that there was a high yield overall of both I-SceI and DR-GFP plasmids (Table 4.3). DR-GFP.3 was the only plasmid with a low DNA yield (93 ng/µl). The purity of these plasmids was high as they all had a 260/280 ratio of ~ 1.8.

4.3.2 Restriction Endonuclease Digestion

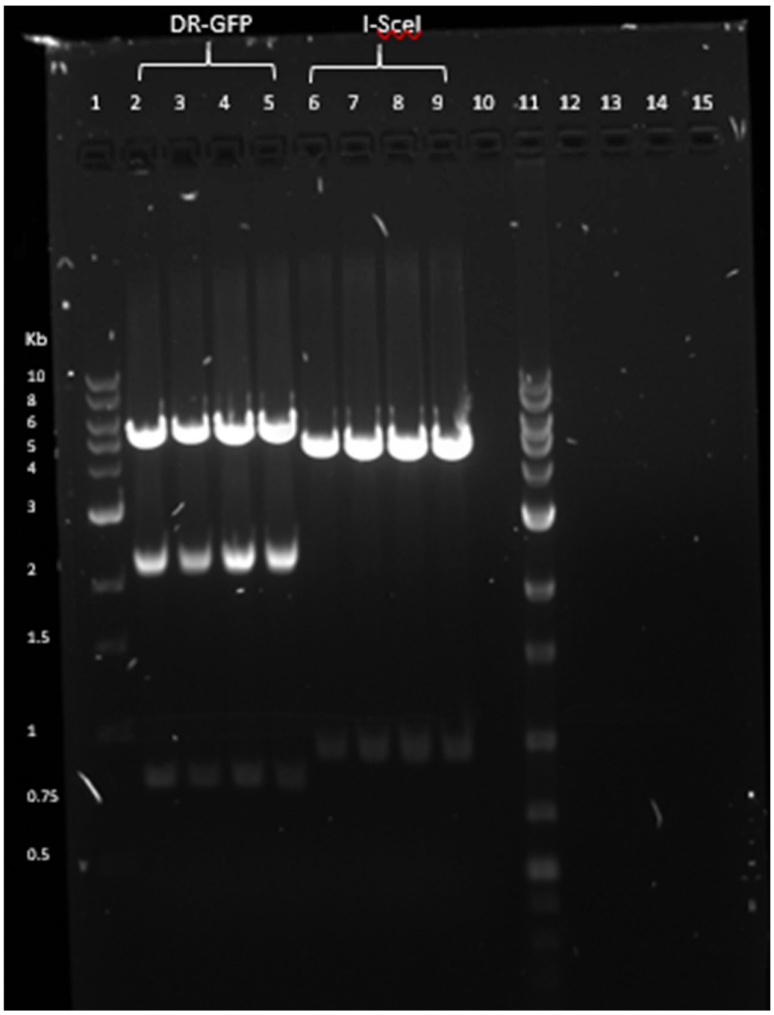

Figure 4.1 Restriction Digest of DR-GFP and I-SceI

From Figure 4.1, lanes 2-5 (DR-GFP) have digested DNA fragment sizes of 5542 bp, 2298 bp, and 806 bp and lanes 6-9 (I-SceI) have digested DNA fragment sizes of 4717 bp and 948 bp. This confirms that the plasmids isolated are DR-GFP and I-SceI.

4.3.3 Puromycin Selection

Over the first week following transfection and puromycin selection, approximately 80% cell death in the DR-GFP1 and DR-GFP2 cultures and 100% cell death in the control culture (which did not contain any plasmid conferring puromycin resistance) was observed. Over the following two weeks, cell numbers increased in the DR-GFP cultures and eventually required passaging. At the end of three weeks, there were three 80% confluent plates per plasmid. Some of these cells were frozen as a backup in case N2a-DRGFP cells contracted a bacterial or yeast infection.

4.4 Discussion

The first objective of this chapter was to extract plasmid DNA and purify it. This was achieved by bacterial transformation of I-SceI and DR-GFP plasmids, and purification by miniprep. The status of these plasmids was confirmed by restriction endonuclease digestion.

The main objective of this chapter was to generate a stable cell line of N2a-DRGFP cells. DR-GFP DNA was transfected into N2a cells by lipofection and the transfected cells were selected for by the addition of puromycin in the growth media for three weeks. DR-GFP has a puromycin resistance gene so only cells with the DR-GFP construct could survive.

This chapter was very important for generating stably integrated DR-GFP in N2a cells. This means that the DR-GFP gene has been integrated into the cell's genome. This is opposed to a transient transfection in which the DNA has entered the cell but is not integrated into the genome. Stable integration allows the cell to replicate the DR-GFP gene, and all descendants will express the gene. This means that a stable cell line of N2a-DRGFP cells can be generated.

After three weeks of puromycin selection, when the cells were assumed to have integrated the DR-GFP plasmid into its genome, some cells were

frozen. This was to ensure that we had N2a-DRGFP cells available if the cells that were being sub-cultured became infected. During the course of the project, the cells contracted a bacterial infection and were all discarded, to prevent other cells in the incubator becoming infected. Bacterial infections are very common in cell lines, due to contamination. Because of this, it was good practice to have stored these cells, so we were able to thaw them out and begin experiments again, without too much delay.

Cells also began to change morphology from small circular cells with very small neurites, to long neurite outgrowth and less circular shape. This could have been due to the very low number of cells that were on the plates during the initial stages of puromycin selection. When N2a cells are low in confluency they have space for neurite outgrowth, compared to in a confluent plate, where there is not much space for this growth. Another reason could have been that the cells were in fact starting to differentiate naturally. As was shown in the EdU experiment (Chapter 2), even in the 10% FBS condition not all cells were proliferative after seven days of cell growth. With the HRR experiment N2a-DRGFP cells will need to be cultured with 1% FBS media and 10 μM RA. These cells will then be tested for by EdU incorporation to determine their proliferative state. Thus, if differentiation was occurring it would not negatively impact this experiment, and could potentially be an aid, as 67% of cells were differentiated with 1% FBS media and 10 μM RA.

Chapter 5

HRR in Proliferating Cells

5.1 Introduction

As a precursor to testing HRR in post-mitotic neuronal cells, experiments in this chapter were carried out to validate the N2a-DRGFP cell line.

The integration of the N2a-DRGFP vector can validated by PCR of the cells. Primers are used that are specific for the DR-GFP vector, so if the plasmid is correct a portion of it will be amplified and the DNA can be visualised on agarose gel. This will confirm that the construct isolated is correct and integration has been achieved.

The validation of I-SceI can be shown by transfection into a stable cell line of proliferating N2a-DRGFP cells. Previous work with HT22 cells has shown that HRR can occur in proliferating neuronal cells. Because of this, I-SceI transfection in proliferating N2a-DRGFP cells should induce a single DSB at the *I-SceI*/Stop recognition site, and successful conversion to a functional GFP sequence could occur.

Once validation of the cell line N2a-DRGFP has occurred, these cells can then be differentiated, using protocol from Chapter 3 and tested for HRR.

5.2 Methods

5.2.1 Transfection of I-SceI into Stable Cell Line

N2a-DRGFP cells were seeded on a 6-well plate with 2 ml of growth media – three wells consisted of DR-GFP1 and three wells consisted of DR-GFP2 (Figure 5.1). Cells were seeded at a confluency of approximately 60% and were left for 24 hours. After 24 hours the confluency was approximately 80%.

Three conditions were used: negative control (no DNA added), GFP positive control (pEGFP plasmid added), and I-SceI (I-SceI plasmid added). Nanodrop reading of pEGFP was done using methods as stated in Chapter 4.2.3 and results from this are included in Chapter 4.3.1.

I-SceI1 and pEGFP were removed from the -20°C freezer. Samples were diluted to a concentration 4.7 µg/ml of DNA by dilution with serum-free media.

The components of each sample is listed below in Table 5.1. There were three lipofectamine samples made in total. Lipofectamine was added to the media slowly and mixed to prevent aggregates from being formed. The DNA samples were added slowly to lipofectamine samples and mixed thoroughly. These samples were left to incubate for 5 minutes.

Components	**Lipofectamine (x3) Tube**	**I-SceI1 Tube**	**pEGFP Tube**	**Control Tube**
Lipofectamine	13.5 µl	-	-	-
DNA	-	21 µl	22 µl	-
Serum-free media	200 µl	200 µl	200 µl	200 µl

Table 5.1 Transfection of N2a-DRGFP with I-SceI, lipofectamine and control samples.

N2a-DRGFP Cells were washed with PBS. Once PBS was removed 200 µl of DNA/lipofectamine/media solution was added to each well to the specifications in Figure 5.1. An additional 1.3 ml of serum free media was added to each well. The cells were placed in the incubator for four hours.

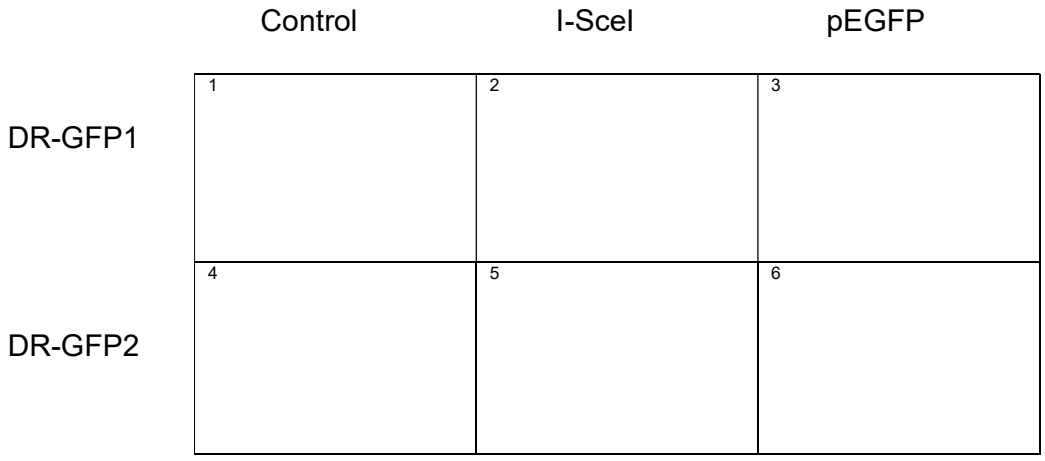

Figure 5.1 6-well plate conditions for transfection of I-SceI and controls into DR-GFP cells

After four hours the media was removed from the cells and growth media was added at 2 ml per well. The cells were then placed back in the incubator.

After 48 hours cells were checked for fluorescence, by confocal microscopy.

5.2.2 Co-Transfection of I-SceI and DR-GFP

Co-transfection is the simultaneous transfection of two DNA plasmids. I-SceI1 and DR-GFP1 were co-transfected into N2a cells.

N2a cells were seeded on a 6- well plate with 2 ml of media. They were seeded at a confluency of approximately 60% and were left for 24 hours. After 24 hours the confluency was approximately 80%.

Three conditions were used – control (no DNA added), GFP positive (pEGFP plasmid added), and I-SceI + DR-GFP (I-SceI1 and DR-GFP1 plasmids added).

I-SceI1, DR-GFP1 and pEGFP were removed from the -20°C freezer. The pEGFP sample was diluted to a concentration 5 µg/ml of DNA by dilution

with serum-free media. I-SceI and DR-GFP were diluted to a concentration of 2.5 µg/ml of DNA by dilution with serum-free media.

The components of each sample is listed below in Table 5.2. There were three lipofectamine samples made in total. Lipofectamine was added to the media slowly and mixed to prevent aggregates from being formed. The DNA samples were then added slowly to lipofectamine samples and mixed thoroughly. These samples were left to incubate for 5 minutes.

Components	**Lipofectamine Tube (x3)**	**I-SceI.1 and DR-GFP1 Tube**	**pEGFP Tube**	**Control Tube**
Lipofectamine	13.5 µl	-	-	-
DNA	-	11.2 µl I-SceI 5.7 µl DR-GFP1	22 µl	-
DMEM media	200 µl	200 µl	200 µl	200 µl

Table 5.2 Components for co-transfection of I-SceI and DR-GFP into N2a cells

Cells were washed with PBS. Once PBS was removed the DNA/ lipofectamine/media solution was added to wells at 200 µl per well as per specifications in Figure 5.2. An additional 1.3 ml of serum free media was added to each well the cells were placed in the incubator for four hours.

After four hours the media was removed from the cells and growth media was added at 2 ml per well. The cells were then placed back in the incubator.

After 48 hours cells were checked for fluorescence, by confocal microscopy.

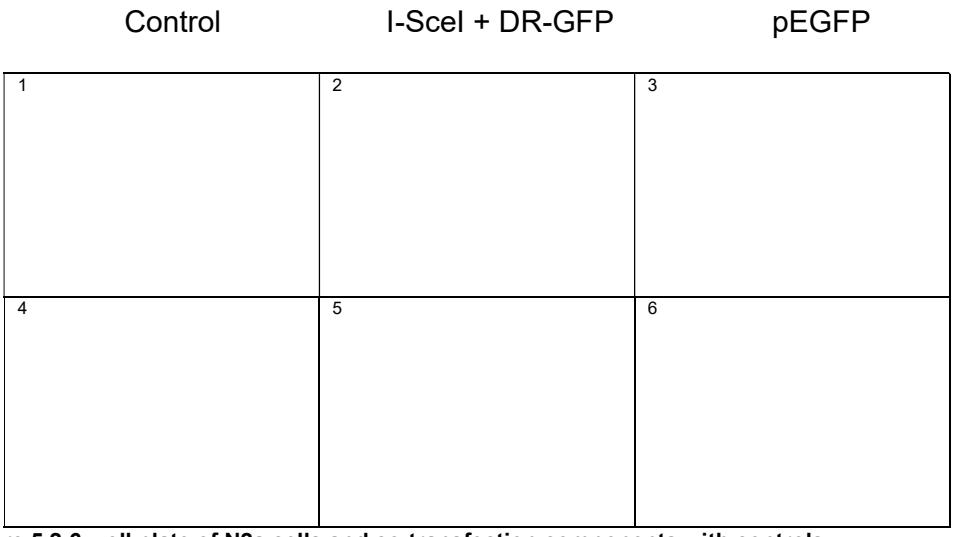

Figure 5.2 6-well plate of N2a cells and co-transfection components with controls.

5.2.3 Confocal Microscopy

The transfection and co-transfection used the same settings on the confocal microscope. After the appropriate incubation time, the 6-well plates were removed from the incubator and taken to the confocal room.

One laser channel was used;

Channel 1 settings:

Dye – EGFP

Voltage – 536 V

Excitation wavelength – 488 nm

Emission wavelength – 509 nm

5.2.4 DNA Extraction

DNA was extracted from N2a-DRGFP cells using the Chelex method [120] to determine its DR-GFP status. The cells were first trypsinised. After cells had dislodged from the flask, 5ml growth media was added, and cells were centrifuged in a falcon tube at 500 x g for 5 minutes. The supernatant was then removed, and the pellet was resuspended in 500 µl of 5% PBS. This

was then transferred into an Eppendorf tube and centrifuged at 500 x g for a further 5 minutes. PBS was removed and 500 µl of 5% Chelex 100 (Bio-Rad) in sterile dH_2O was added to the Eppendorf tube. The tube was heated to 99°C for 10 minutes in the thermomixer. Once removed it was centrifuged for 5 minutes at 500 x g. The supernatant was then transferred to another Eppendorf tube and the pellet discarded.

5.2.5 Polymerase Chain Reaction

The N2a-DRGFP status of the cells was determined by polymerase chain reaction (PCR) and was visualised on an agarose gel. Two sets of primers were used: EGFP-C / PuroF and pCAG-F / EGFP-C-R. These two sets of primers both amplify the forward and reverse of the DR-GFP insert. EGFP-C/PuroF amplifies 1074 bp and pCAG-F/EGFP-C-R amplifies 1033 bp. The sequence of the primers are stated in Table 5.5.

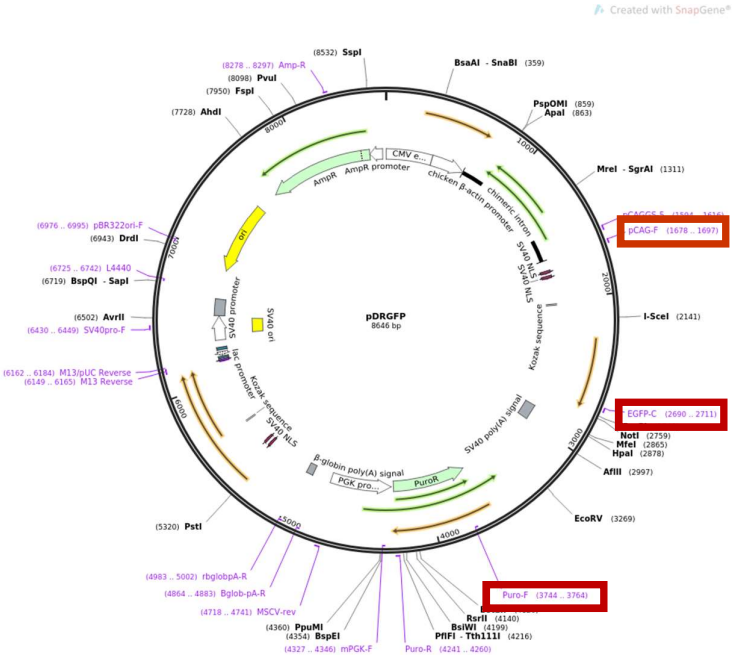

Figure 5.3 Plasmid map of pDRGFP and the primers used for PCR to determine N2a-DRGFP status; pCAG-F, EGFP-C, EGFP-C-R, and Puro-F

Reaction Components	Single PCR Reaction	Master Mix (x2)
10x PCR Buffer	2.5 µl	10 µl
Primer 1	0.5 µl	2 µl
Primer 2	0.5 µl	2 µl
DNA	5 µl	-
MgCl	2 µl	8 µl
dNTPs	2.5 µl	10 µl
H_20	11.75 µl	47 µl
Taq Polymerase	0.25 µl	1 µl

Table 5.3 Components for PCR to determine N2a-DRGFP status of cells.

Two separate master mixes were made up to the specifications in Table 5.3. The first master mix contained the primers EGFP-C / PuroF and the second master mix contained the primers pCAG-F / EGFP-C-R. These primers were all used at a working concentration of 30 pmol/µl. From the master mixes, 20 µl was added into PCR tubes (4 tubes per master mix). DNA was then added to each tube according to the specifications in Table 5.4.

Conditions for PCR – DNA and primers used for each sample
1. No DNA / EGFP-C / PuroF
2. DR-GFP1 / EGFP-C / PuroF
3. DR-GFP2 / EGFP-C / PuroF
4. Plasmid DNA / EGFP-C / PuroF
5. No DNA / pCAG-F / EGFP-C-R
6. DR-GFP1 / pCAG-F / EGFP-C-R
7. DR-GFP2 / pCAG-F / EGFP-C-R
8. Plasmid DNA / pCAG-F / EGFP-C-R

Table 5.4 Conditions used for PCR (DNA and primers used) to determine N2a-DRGFP status of cells.

Primers	Sequence	Annealing Temp (°C)	Length (bases)
EGFP-C	CATGGTCCTGCTGGAGTTCGTG	61	22
PuroF	GCAACCTCCCCTTCTACGAGC	60	21
pCAG-F	GCAACGTGCTGGTTATTGTG	57	20
EGFP-C-R	CACGAACTCCAGCAGGACCATG	60	22

Table 5.5 Primers used for PCR to determine N2a-DRGFP status of cells.

The PCR conditions were as follows:

1. 94°C for 3 mins for initial denaturing of the DNA, and to activate the Taq DNA polymerase (Invitrogen)
2. 35 cycles of:
    a. 94°C for 30 secs (Denaturing)
    b. 62°C for 30 secs (Annealing)
    c. 72°C for 30 secs (Elongation)
    d. Final elongation at 72°C for 2 mins
3. Hold at 4°C indefinitely

The resulting product was then analysed by agarose gel electrophoresis.

5.2.5.1 Agarose Gel Electrophoresis

A 1% agarose gel was made as per specifications in Chapter 2.5. Gel loading buffer was added to each sample. A 5 kb ladder was added to the first lane. The samples were then added to the lanes. The gel was run at 70 V for 1 hour.

Gels were imaged by ethidium bromide fluorescence using a UV gel documentation system (Image Quant LAS 400). The PCR amplification product from the EGFP-C / PuroF primer combination would be expected to be 1074 bp, while the PCR amplification product from the pCAG-F / EGFP-

C-R primer combination would be expected to be 1033 bp. These DNA amplifications can be seen on a gel and determine if the products were correct.

5.2.6 Sequencing of Plasmid DNA

Plasmids DR-GFP1, DR-GFP2, I-SceI1, and I-SceI2 were sent to the University of Waikato Sequencing Facility for sequencing. The plasmids were diluted with dH_2O to a final concentration of 150 ng/µl. The primers used are stated in Table 5.6 and Table 5.7. These primers were given at a concentration of 5 pmol/µl.

I-SceI Primers			
Primer Name	**Sequence 5' to 3'**	**Annealing Temp (°C)**	**Length (bases)**
pCAG-F	GCAACGTGCTGGTTATTGTG	57	20
Bglob-pA-R	TTTTGGCAGAGGGAAAAAGA	61	20

Table 5.6 Primers for I-SceI

pDR-GFP Primers			
Primer Name	**Sequence 5' to 3'**	**Annealing Temp (°C)**	**Length (bases)**
pCAG-F	GCAACGTGCTGGTTATTGTG	57	20
EGFP-C-R	CACGAACTCCAGCAGGACCATG	60	22

Table 5.7 Primers for DR-GFP

5.2.6.1 Plasmid Maps

Figure 5.4 pDRGFP vector map with primers pCAG-F and EGFP-C-R highlighted

The pDR-GFP primers, pCAG-F and EGFP-C-R amplified a section of the DNA that contained the I-SceI recognition site (Figure 5.4). The EGFP-C-R primer is a reverse primer and pCAG-F is a forward primer. In Figure 5.4 the EGFP-C primer is the forward primer of EGFP-C-R.

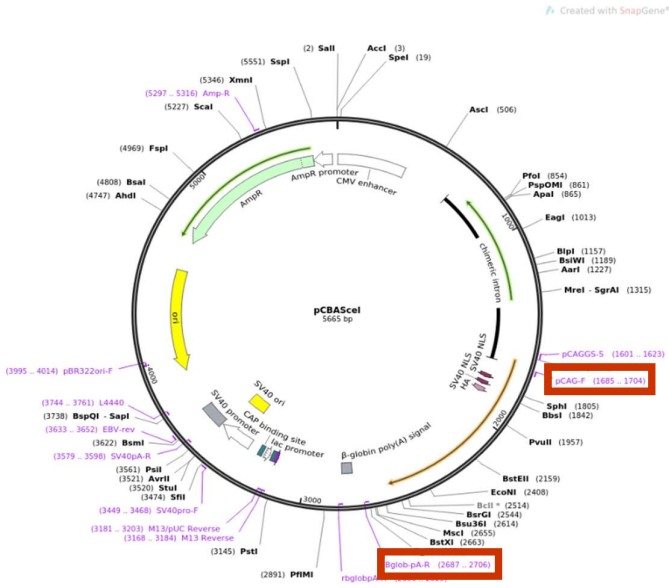

Figure 5.5 pCBAScel vector map, with primers pCAG-F and Bglob-pA-R highlighted

The I-SceI primers, pCAG-F and Bglob-pA-R amplified a section of the DNA that contained that contains the ORF (Figure 5.5). pCAG-F is the forward primer and Bglob-pA-R is the reverse primer.

Once the results from sequencing were received, they were analysed on Geneious Prime. All electropherograms of sequences were captured and analysed. The reverse primer sequences were reverse complemented. After each sequence was analysed, they were mapped to the plasmid references (Figures 5.4 and 5.5) to determine if the sequences were correct.

The sequences were also put through BLAST software, using BLASTn to find similar sequences.

5.3 Results

5.3.1 Transfection of I-SceI into Stable Cell Line

<table>
<tr><td>No GFP control</td></tr>
<tr><td> 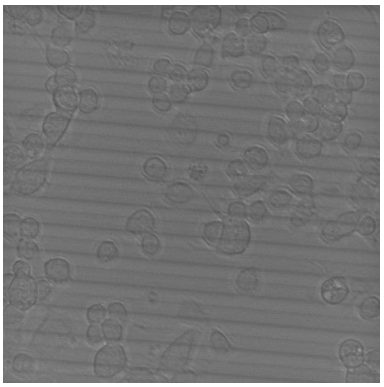
A</td></tr>
<tr><td>Transfection of DR-GFP and I-SceI into N2a cells</td></tr>
<tr><td> 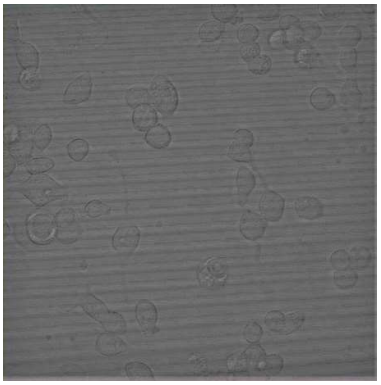
B
 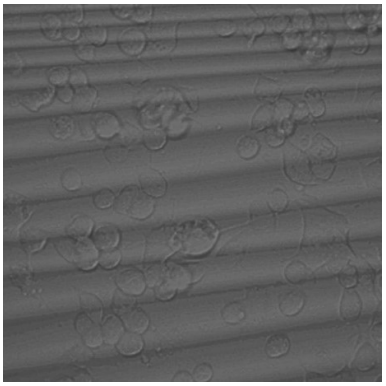
C</td></tr>
<tr><td>pEGFP transfected N2a cells</td></tr>
<tr><td> 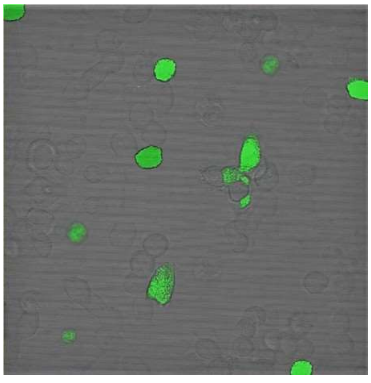
D</td></tr>
</table>

Table 5.8 Images of N2a-DRGFP cells from transfection of I-SceI

Transfection of I-SceI into N2a-DRGFP cells did not show any fluorescence (Table 5.8, Image B and C). Transfection of I-SceI has been shown to occur, as the control plasmid pEGFP was successfully transfected into N2a-DRGFP cells, as shown by green fluorescence (Table 5.8, Image D). The control of no DNA did not show any fluorescence (Table 5.8, Image A), which shows there was no contamination and that no spontaneous GFP conversion had occurred in the N2a-DRGFP cells.

There are three different reasons why N2a-DRGFP cells may not have shown fluorescence and these are: that HRR does not occur in proliferating N2a neuronal cells; that the I-SceI plasmid is not functional; or cells have not been stably transfected and do not contain DR-GFP.

5.3.2 Co-Transfection of I-SceI and DR-GFP into N2a cells

No GFP control
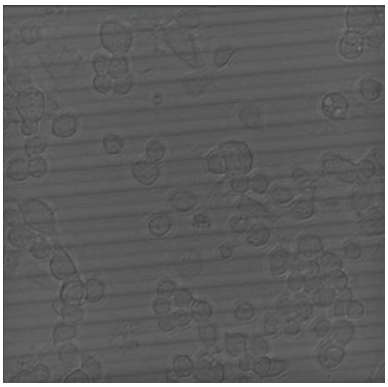 A
Co-Transfection of DR-GFP and I-SceI into N2a cells
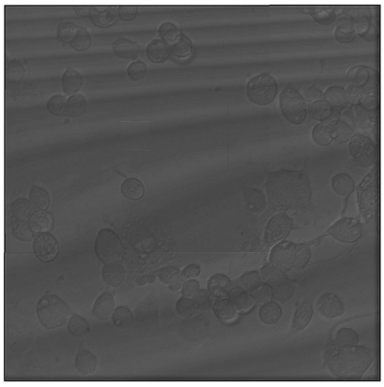 B
pEGFP transfected N2a cells
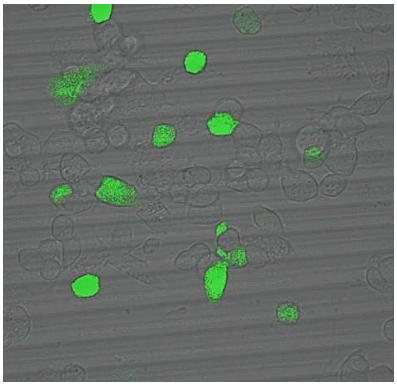 C

Table 5.9 Images of N2a cells from co-transfections with DR-GFP and I-SceI

Co-transfection of I-SceI and DR-GFP into N2a cells did not show any fluorescence (Table 5.9, Image B). Transfection of I-SceI and DR-GFP has been shown to occur, as the control plasmid pEGFP was successfully transfected into N2a cells, as shown by green fluorescence (Table 5.9, Image C). The control of no DNA did not show any fluorescence (Table 5.9, Image A), which shows there was no contamination.

There are three different reasons why N2a cells may not have shown fluorescence and these are: that HRR does not occur in proliferating N2a neuronal cells; that the I-SceI plasmid is not functional; or the DR-GFP plasmid is not correct.

5.3.3 Sequencing of I-SceI

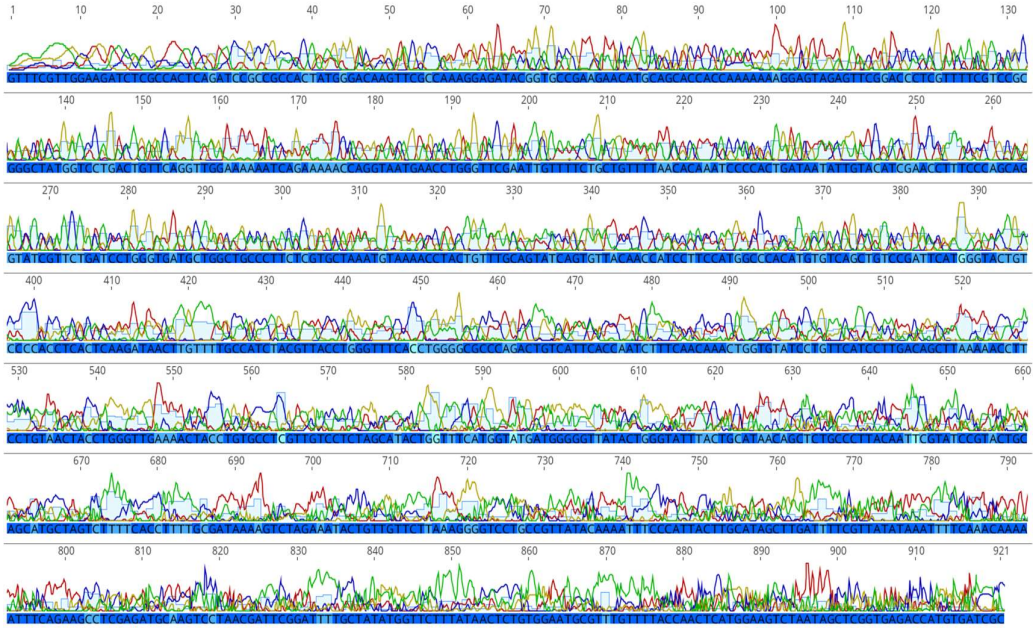

Figure 5.6 Electropherogram of I-SceI1. Primer pCAG-F

Figure 5.6 shows the electropherogram of I-SceI1 sequence from the primer pCAG-F. This sequence lacks distinct, single lined peaks in most areas which shows that the sequence is not of high quality. The data shows overlapping, jagged peaks, which means that the base calls that have been given to this sequence from the software are no longer reliable.

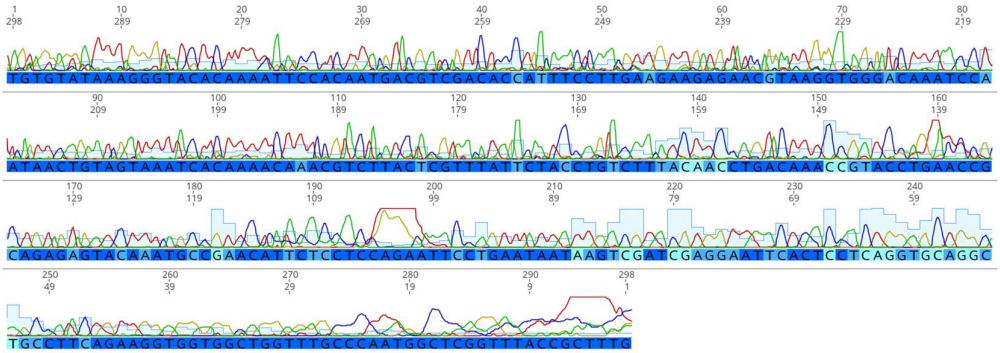

Figure 5.7 Electropherogram of I-SceI1. Primer Bglob-pA-R. Sequence has been reverse complemented

Figure 5.7 shows the electropherogram of I-SceI1 sequence from the primer Blgob-pA-R. This sequence has more distinct and singled lined peaks and less contamination and artifacts than the electropherogram of I-SceI1 with the pCAG-F primer. This means that this sequence is of better quality than the pCAG-F primer. Data at the start and end of the sequence is of low quality, which is to be expected.

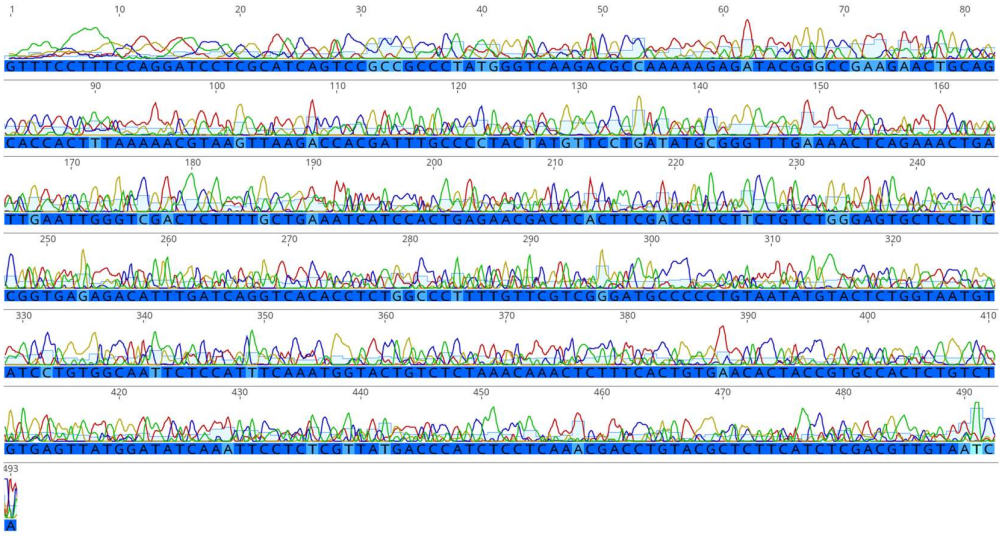

Figure 5.8 Electropherogram of I-SceI2. Primer pCAG-F.

Figure 5.8 shows the electropherogram of I-SceI2 sequence from the primer pCAG-F. This sequence lacks distinct, single lined peaks in most areas, which shows that the sequence is not of high quality. The data shows overlapping, jagged peaks, which means that the base calls that have been

given to this sequence from the software are no longer reliable.

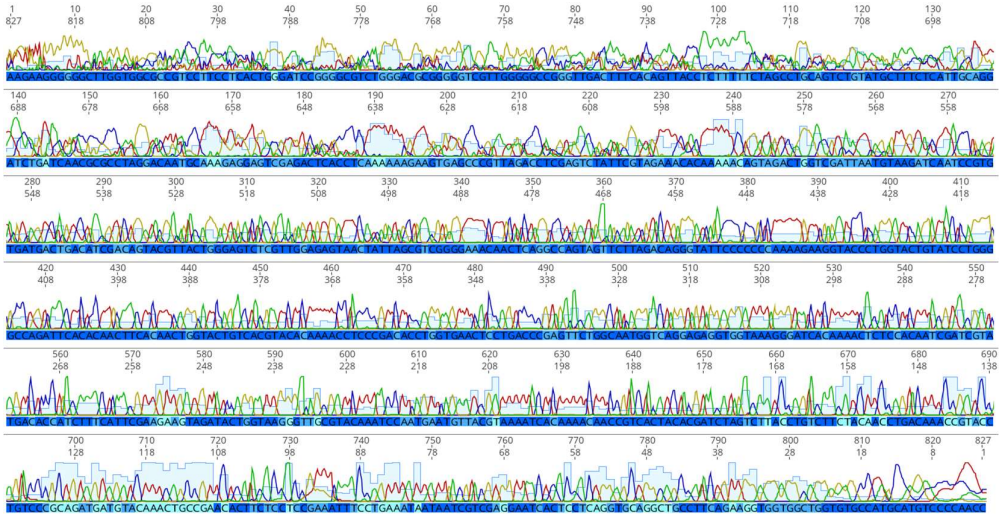

Figure 5.9 Electropherogram of I-SceI2. Primer Bglob-pA-R. Sequence was reverse complemented.

Figure 5.9 shows the electropherogram of I-SceI2 sequence from the primer Blgob-pA-R. This sequence has more distinct and singled lined peaks and less contamination and artifacts than the electropherogram of I-SceI2 with the pCAG-F primer. This means that this sequence is of better quality than the pCAG-F primer. Data at the start and end of the sequence is of low quality, which is to be expected.

5.3.3.1 I-SceI Mapped to pCBAScel

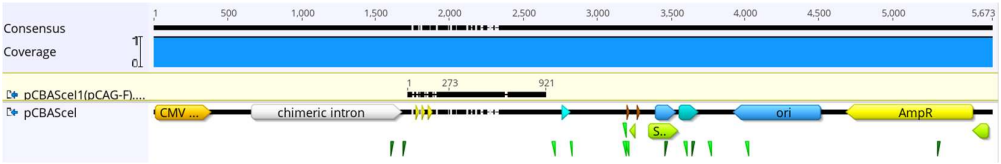

Figure 5.10 I-SceI1 sequence from pCAG-F primer mapped to pCBAScel plasmid

Figure 5.10 shows that the I-SceI1 sequence from the PCAG-F primer was able to be mapped to the reference sequence pCBAScel. The I-SceI1 sequence runs from approximately 1750 bp to 2600 bp on the pCBAScel

reference sequence. This shows that the I-SceI1 sequence that we have is correct as the pCAG-F primer binds to I-SceI at 1685-1704 bp.

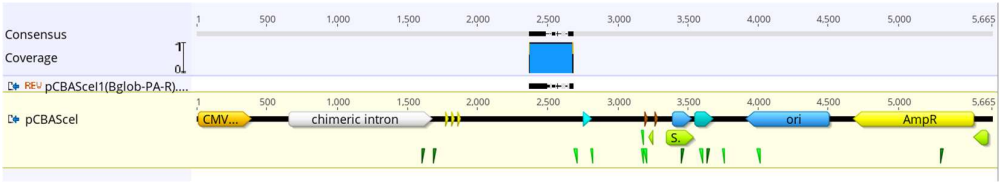

Figure 5.11 I-SceI1 sequence from Bglob-pA-R primer mapped to pCBAScel plasmid

Figure 5.11 shows that the I-SceI1 sequence from the Bglob-pA-R primer, which has been reverse complemented, was able to be mapped to the reference sequence pCBAScel. The I-SceI1 sequence runs from approximately 2400 bp to 2700 bp on the pCBAScel reference sequence. This shows that the I-SceI1 sequence that we have is correct as the Bglob-pA-R primer binds to I-SceI at 2687-2706 bp.

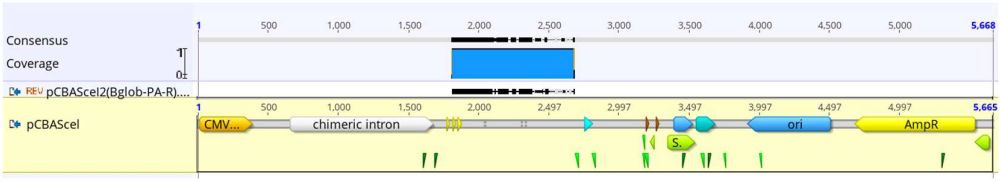

Figure 5.12 I-SceI2 sequence from Bglob-pA-R primer mapped to pCBAScel plasmid

Figure 5.12 shows that the I-SceI2 sequence from the Bglob-pA-R primer, which has been reverse complemented, was able to be mapped to the reference sequence pCBAScel. The I-SceI1 sequence runs from approximately 2400 bp to 2700 bp on the pCBAScel reference sequence. This shows that the I-SceI1 sequence that we have is correct as the Bglob-pA-R primer binds to I-SceI at 2687-2706 bp.

The I-SceI2 sequence from the primer pCAG-F was not able to be mapped to the reference sequence. This could have been due to the poor quality of DNA reads that were obtained. Overall, the pCAG-F primed sequences resulted in lower quality reads than the Bglob-pA-R primed sequence reads.

5.3.4 Sequencing of DR-GFP

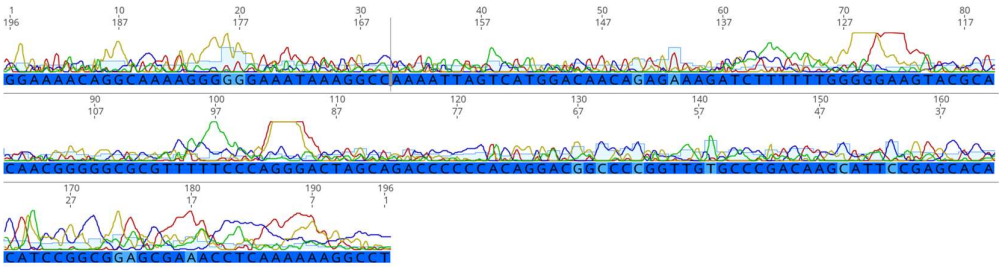

Figure 5.13 Electropherogram of DR-GFP1. Primer EGFP-C-R.

Figure 5.13 shows the electropherogram of DR-GFP1 sequence from the primer EGFP-C-R. This sequence lacks distinct, single lined peaks in most areas which shows that the sequence is not of high quality. The data shows overlapping, jagged peaks, which means that the base calls that have been given to this sequence from the software is no longer reliable.

There was no sequence read for DR-GFP1 with the primer pCAG-F.

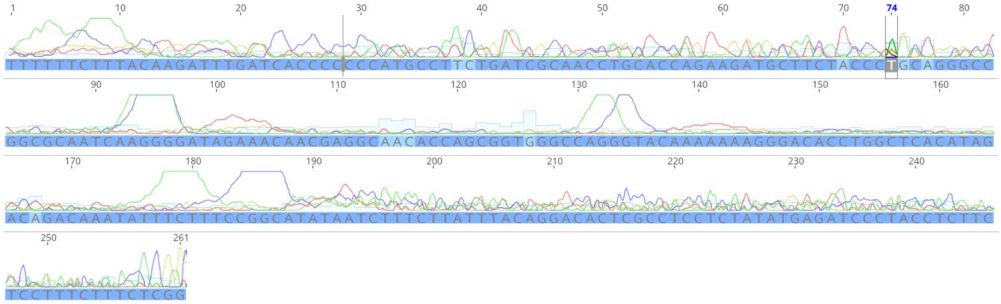

Figure 5.14 Electropherogram of DR-GFP2. Primer pCAG-F.

Figure 5.14 shows the electropherogram of DR-GFP2 sequence from the primer pCAG-F. This sequence lacks distinct, single lined peaks in most areas which shows that the sequence is not of high quality. The data shows overlapping, jagged peaks, which means that the base calls that have been given to this sequence from the software is no longer reliable. There is also a lack of steep peaks which shows that there is a lack of DNA reads for each base.

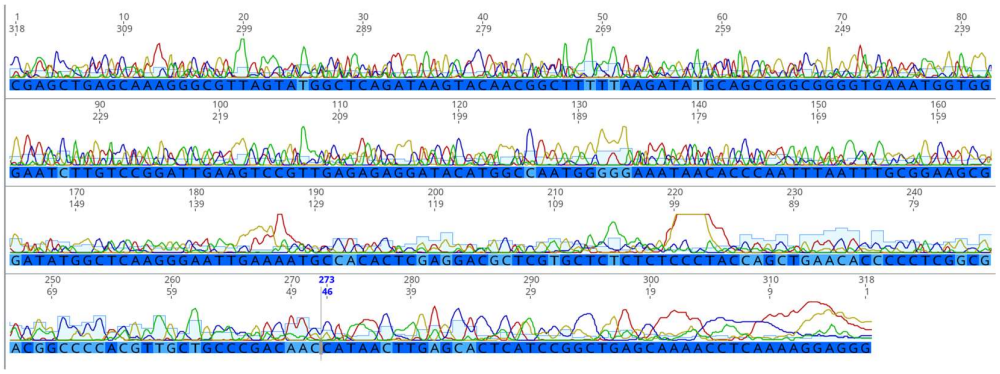

Figure 5.15 Electropherogram of DR-GFP2. Primer EGFP-C-R.

Figure 5.15 shows the electropherogram of DR-GFP2 sequence from the primer EGFP-C-R. This sequence lacks distinct, single lined peaks in most areas which shows that the sequence is not of high quality. The data shows overlapping, jagged peaks, which means that the base calls that have been given to this sequence from the software is no longer reliable.

DR-GFP1 and DR-GFP2 were not able to be mapped to the reference sequence which shows that the plasmids that we had were not pDRGFP.

5.3.5 PCR Products

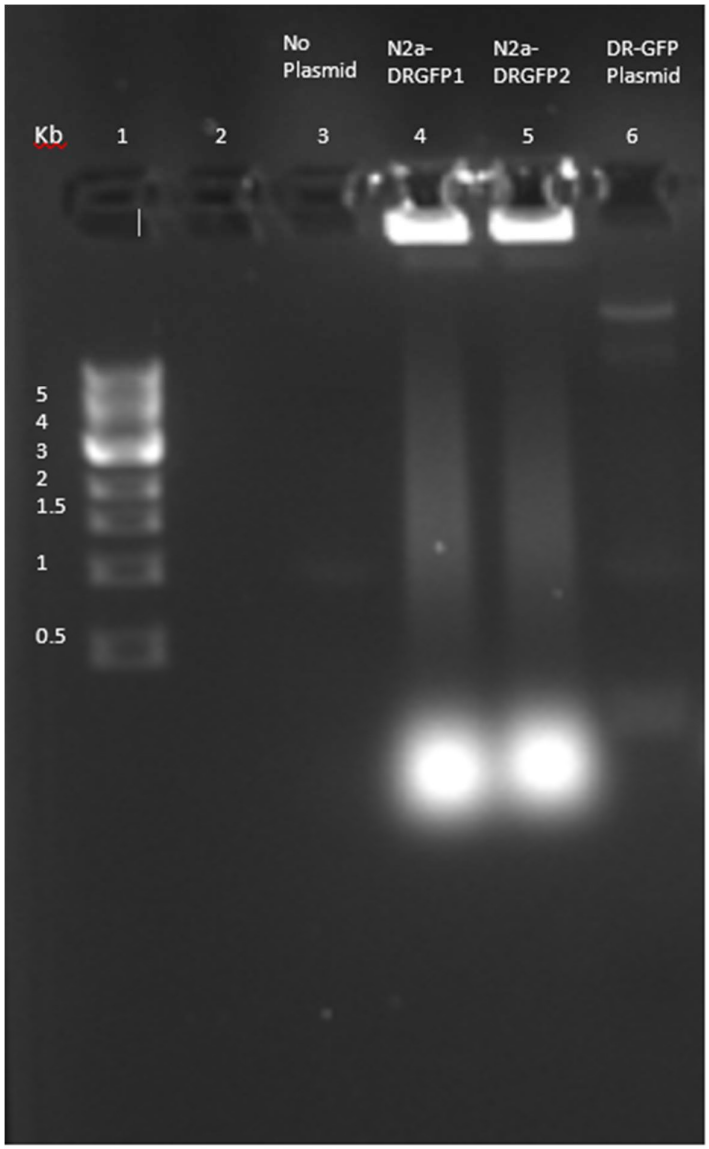

Figure 5.16 1% Agarose gel. PCR products of N2a-DRGFP cells with EGFP-C-R and pCAG-F primers. Controls used are no Plasmid DNA and DR-GFP plasmid.

From Figure 5.16, it can be seen that DR-GFP1 and DR-GFP2 (lane 4 and 5) have not been amplified. The no DNA control (lane 3), which was a negative control has not been amplified, which shows that there is no contamination. The DR-GFP plasmid (lane 6), which is a positive control has not been amplified. Amplification of pCAG-F/EGFP-C-R should have been 1074 bp. This PCR shows that N2a cells had not been stably integrated with DR-GFP1 or DR-GFP2. It also suggests that the DR-GFP

plasmid that has been isolated may not be correct. Because N2a had not been stably integrated with DR-GFP, it offers an explanation on why the transfection of N2a-DRGFP cells with I-SceI did not work.

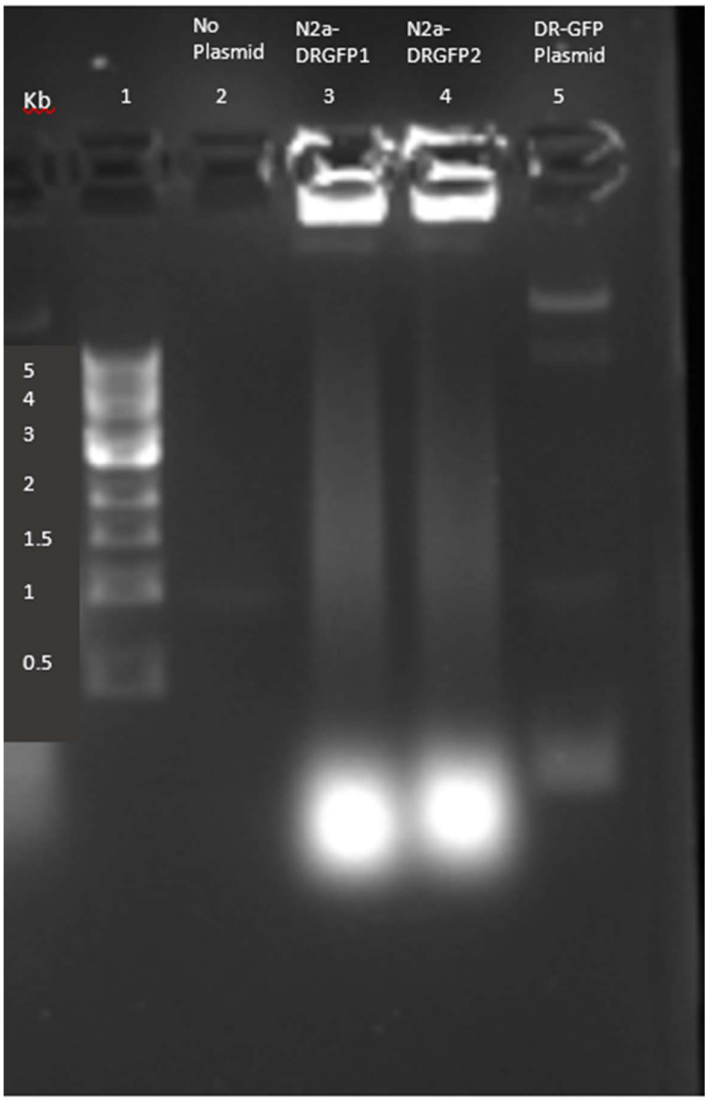

Figure 5.17 1% Agarose gel. PCR products of N2a-DRGFP cells with Puro-F and primers. Controls used are no Plasmid DNA and DR-GFP plasmid.

From Figure 5.17, it can be seen that DR-GFP1 and DR-GFP2 (lane 3 and 4) have not been amplified. The no DNA control (lane 2), which was a negative control has not been amplified, which shows that there is no contamination. The DR-GFP plasmid (lane 5), which is a positive control has not been amplified. Amplification of Puro-F/EGFP-C should have been

1033 bp. This PCR shows that N2a cells had not been stably integrated with DR-GFP1 or DR-GFP2. It also suggests that the DR-GFP plasmid that has been isolated may not be correct.

The PCR reactions show that N2a had not been stably integrated with DR-GFP. Because this integration did not occur, it offers an explanation on why the transfection of N2a-DRGFP cells with I-SceI did not work. The plasmid DNA used as a positive control was not amplified either, which suggests that the plasmid that was isolated was not DR-GFP.

5.4 Discussion

The objective of this chapter was to validate the N2a-DRGFP cell line, through validation of the integration of the DR-GFP construct into N2a cells and also through the validation of *I-SceI* to cause a DSB at the *I-SceI*/Stop recognition site and successful conversion to a functional GFP coding sequence. It was expected that because previous work with HT22-pDRGFP cells showed HRR, that this experiment would too. However, the results from the HRR assay in proliferating N2a-DRGFP cells did not show any green fluorescence.

There are many possible reasons behind this experiment being unsuccessful, the first being that HRR does not occur in neuronal cells. However, as these cells were still proliferating, and we have previous data showing that HRR can in fact occur in dividing HT22-pDRGFP neuronal cells, this does not seem likely.

The storage of these cells could have also affected the results. The storage conditions of these cells are supposed to be in liquid nitrogen vapor phase – however, the best storage possible at our facility is a -80°C freezer. This storage could have led to a lower viability of cells, which meant that the cells took longer to grow and further increased the passage number.

The passage number could have affected this experiment. These cells were gifted to us from Dr Greg Jacobson, who had received them ten years prior. They were kept at -80°C for those ten years, before being thawed in February 2019. The passage number was not known to him when they were received, so it could be extremely high by the time we got to the HRR experiment. Studies show [121-126], that the passage number can affect the cellular productivity, protein yields, morphology, transfection efficiency, and growth rates of cells. However, because the pEGFP control was able to be transfected into cells, it seems unlikely that this is the reason why the experiment was unsuccessful. New cells were also thawed out and the co-transfection was repeated, and results were still negative.

Another possibility is that N2a cells are deficient for HRR. Because N2a cells are a neuroblastoma cell line, it could be a possibility that it is deficient for some repair processes. From searching literature, there was one paper that showed that transgene knock-in in N2a cells was achieved thorough homology-mediated end joining (HMEJ) and HRR [127]. This evidence suggests that the HRR pathway is not defective in N2a cells.

Another possibility is that I-SceI was not transfected or the plasmid was incorrect. In the transfection experiments the pEGFP plasmid was used as a control to confirm that the plasmids were transfected into the N2a cells. I-SceI was also sent away for sequencing and the results from sequencing showed that the plasmid was correct, as the sequences could be mapped to the reference plasmid.

The next possibility is that the N2a cells were not stably transfected with DR-GFP. PCR of the N2a-DRGFP cell lines can show if DR-GFP has been integrated into N2a cells. The primers that were ordered for PCR to determine N2a-DRGFP status took a long time to be delivered. Because of this, after puromycin treatment, we started further experiments before determining whether DR-GFP had been stably integrated into N2a cells. We assumed because we treated with puromycin for three weeks, that all the

cells that did not contain a puromycin resistance gene would die and we would only be left with N2a cells that contained the DR-GFP construct.

After the unsuccessful experiments in which I-SceI was transiently transfected into N2a-DRGFP cells, co-transfection of I-SceI and DR-GFP was attempted. In the case that integration was not achieved, this approach removed the need for the stable genomic integration of DR-GFP in the N2a cell lines. The pEGFP plasmid, which was a positive control, was transfected into cells and was shown by green fluorescence. The co-transfection of I-SceI and DR-GFP did not show any fluorescence. This supports the idea that the DR-GFP plasmid might not be correct.

When the primers arrived, a PCR of N2a-DRGFP cells was performed to determine whether DR-GFP was indeed in the N2a cells. This PCR did not show any amplification of the DR-GFP-targeted sequence, which suggests that cells were not stably integrated with DR-GFP. There was also no observed amplification of the DR-GFP plasmid, which was used as a positive control, which this suggests that the DR-GFP plasmid may not have been isolated.

If the cells did not contain the DR-GFP plasmid, why did the restriction endonuclease map show DNA with the same cut sizes as DR-GFP? Moreover, how were they selected for in puromycin selection? To answer this question, the purified DR-GFP1 and DR-GFP2 plasmids were sent for sequencing. The results from sequencing showed that the plasmids were not DR-GFP as the obtained sequence could not be mapped to the reference DR-GFP plasmid sequence. In fact, we were not able to find any BLAST hits for the plasmid. However, both the DR-GFP1 and DR-GFP2, obtained from two independent transformed bacterial colonies, were identical in sequence. It is also probable that the plasmid we isolated had a puromycin resistant gene, as it provided resistance to puromycin during N2a selection.

Overall, the result is very surprising as we had selected four independent colonies and all four had the same restriction endonuclease fragment pattern, which were consistent with the fragment sizes expected from a *HindIII* digestion of DR-GFP. In hindsight sequencing should have been done at the same time as the restriction endonuclease digestion; however, because the result was positive, and the primers for sequencing had not arrived at that time, we decided to move on with experiments. The plasmid had been sourced from New York and it seems likely that the lab who had sent us the plasmid did not send the correct one, through possible mislabelling or human error.

Because the results we yielded from this project were negative, the next step would be to first obtain the correct DR-GFP plasmid; which is available through Addgene. After this, a stable cell line of N2a-DRGFP cells could be generated using the same protocol already established (Chapter 4). The differentiation protocol for this experiment has also been established (Chapter 3), in which a non-proliferative state can be achieved in the majority of N2a-DRGFP cells by 1% FBS media and 10 μM RA over the course of seven days, changing the media every three days. Once a non-proliferative state is achieved, the cells could be transiently transfected with I-SceI using the established protocol (Chapter 5.2.1). EdU incorporation and DAPI staining protocol (Chapter 3.2.1.3) would be used in combination to show that cells are non-proliferative and cell viability. The cells could then be viewed by confocal microscopy to determine if HRR in post-mitotic neuronal cells occurs – this would be shown by green fluorescence in a blue stained cell. The lack of red fluorescence would show that the cell is non-proliferative.

Chapter 6

Final Discussion

It is believed that when post-mitotic neurons are subjected to a DNA DSB, the repair pathway used will be the NHEJ pathway [7, 11, 18]. This pathway is highly inaccurate and can lead to the loss of very important information and accumulation of DNA lesions [11, 36]. Neurons are subjected to large amounts of DNA damage in every cell, each day, due to its high metabolic activity [41]. Neurons cannot replace themselves if they are lost, so it seems critical that a high-fidelity repair process, such as HRR, should be used to protect the integrity of these cells, as they must last a lifetime. The goal of this project was to determine whether HRR, a highly accurate repair process for DSBs, occurs in post-mitotic neuronal cells. The neuroblastoma cell line N2a was used to determine if HRR occurs in post-mitotic neuronal cells. The results did not show that HRR occurred in neurons.

From this project, a differentiation protocol was established. A post-mitotic state can be induced in N2a cells by treatment with 1% FBS media and 10 μM RA over the course of seven days. The lack of cell division and DNA synthesis in cells was determined by cell count and EdU incorporation.

Next, DR-GFP and I-SceI plasmids were purified by miniprep techniques and concentrations were determined by nanodrop. The status of plasmids was determined by restriction endonuclease digestion. DR-GFP1 and DR-GFP2 were transfected into proliferating N2a cells to produce N2a-DRGFP.1 and N2a-DRGFP.2, respectively, and puromycin selection was used to obtain stably integrated lines. Once the N2a-DRGFP cell line was established, the cells were transfected with I-SceI to create a single DSB in the *I-SceI*/Stop recognition site in the DR-GFP vector. If HRR was to occur the homologous sequence on the vector would be used and the non-functional GFP protein would be repaired and green fluorescence would be seen by immunofluorescence. However, we were not able to observe

fluorescence. A PCR of N2a-DRGFP cells showed that DRGFP was not stably integrated into N2a cells.

Co-transfections of I-SceI and DR-GFP into N2a cells also did not show any fluorescence. This suggested that the plasmids that were purified may not have been correct.

Sequencing of I-SceI showed that the plasmid was correct. However, sequencing of DR-GFP showed that we did not have the correct plasmid. Because the plasmid was found to be incorrect, no further experiments could be carried out until the correct plasmid is obtained.

6.1 Future Directions

Because the DR-GFP plasmid was incorrect the next step would be to obtain the correct DR-GFP plasmid and use the protocol that we have established from this project to produce a stable cell line of N2a-DRGFP cells that can be differentiated and tested for HRR repair. Unfortunately, due to time constraints it was not possible to obtain the DR-GFP plasmid. However, because HRR of DR-GFP following *I-SceI* cleavage has been shown in proliferating neuronal HT22 cells, it is hypothesised that the N2a cell line will yield similar results.

Moving forward, if HRR is shown to be successful in non-proliferative N2a-DRGFP cells, there are further experiments that can be done to add to the evidence that HRR occurs in post-mitotic neurons, such as use of other cells lines.

6.1.1 Cell Lines

Because N2a cells are an immortalised neuroblastoma cell line, the experimental results from using these cells may not always represent what happens *in vivo*. However, there are advantages of using a cell line which include: that they are relatively easy to culture; they give rise to almost an unlimited number of cells; and they are easy to transfect [128]. With N2a

cells in particular, one of the biggest positives is that they are able to be differentiated. While we did not confirm a differentiated neuronal phenotype using neural-specific antibody markers, our EdU incorporation experiments showed we could induce a non-proliferative state in the majority of cells. These results suggest the N2a cell line will be a good cell line to use once the correct DR-GFP plasmid is obtained.

Cell lines are used before *in vivo* or *ex vivo* experiments to test hypotheses and show they have merit. However, cell lines can have drastically different physiological features from the primary cell type in which they were derived, and manipulations may have occurred to obtain a neuronal phenotype due to the addition of certain growth factors [128].

The use of a primary culture is another option moving forward. Primary cultures are much more reliable as they are not derived from tumours or transformed cells, and as such, they better reflect what occurs *in vivo*. However, there are also disadvantages of using primary cultures, such as they are much more difficult to culture, only a small quantity of cells can be grown, and the transfection efficiency is greatly reduced compared to that of cell lines [128]. It should also be noted that the use of primary cultures requires ethics approval which can take some time to obtain. The use of a primary culture would be the next step after showing that HRR can occur in non-proliferative N2a cells.

To obtain primary neuronal cultures, it would be crucial to engineer mice that contain the DR-GFP vector in their DNA. These cells could then be harvested and transfection with I-SceI could occur. By using a primary neuronal cell culture, it would be possible to definitively establish whether HRR occurs in post-mitotic cells after a DSB.

6.2 Possible Mechanism for HRR in Post-Mitotic Cells

It has been long believed that HRR can only occur in the G2/M and S phase of the cell cycle, where a sister chromatid is present to act as a homologous

sequence for repair. However, there has recently been an influx of publications [18, 129-132] that show that RNA templates could be used as a homologous sequence for HRR. This evidence could provide a mechanism in which post-mitotic neuronal cells are able to use HRR to repair DSBs.

HRR has typically be known to occur between two homologous DNA sequences; however, HRR can occur in RNA sequences, as has been shown through RNA viruses [129]. Research has also shown that synthetic RNA oligonucleotides (oligos) are able to template DSB repair in yeast and human cells [130, 131]. More recently, endogenous transcript RNA has been implicated as a possible template for HRR in yeast *Saccharomyces cerevisiae* [132].

This would mean that cells do not necessarily need to be in a certain phase of the cell cycle to repair DNA DSBs by HRR. Neurons are in the G0 or G1 phase of the cell cycle as they are post-mitotic. However, they are extremely active cells which accumulate up to 50 DSBs in each cell, every day [41]. Because of this large amount of DNA damage that occurs, and the fact that neurons need to last a lifetime, this evidence of RNA templated DNA DSB repair by HRR could be the mechanism in which neurons repair their DNA to a high fidelity. This repair could prevent insertions, deletions, and translocations of extremely important coding information [11, 36]. DNA lesions would also be less likely to accumulate with such an accurate repair process.

This evidence supports our hypothesis that HRR can occur in post-mitotic neuronal cells.

6.3 HDAC Inhibition

There is a large body of evidence that shows that a defective or ineffective repair pathway for DSBs can contribute to neurological and

neurodegenerative pathologies. Because of this, it seems crucial that a high-fidelity repair pathway is used.

If HRR occurs in non-proliferative neuronal cells, it might be possible to enhance the HRR response by the use of HDAC inhibitors. HDAC inhibition is an approach that is an active area of research in the amelioration of neurodegenerative diseases. This is achieved by targeting HDAC activity via small molecule inhibitors, which allows DNA marks to be accessible for DNA repair factors to bind and repair DNA. This approach, however, can often be toxic and can lead to instability of the genome.

The role of H4K16 is extremely important in the DSBR. The acetylation of H4K16 is linked to the HRR pathway. A possible therapeutic for neurodegeneration, could be to increase the acetylation of H4K16 by the inhibition of HDAC activity. There are a number of HDACs that have been targeted to deplete their acetylation activity and a few of these include; HDAC1, HDAC2, HDAC3, and HDAC6 [8, 51, 133-137].

After a DSB, HDAC1 and HDAC2 are rapidly recruited to DNA damage sites where they deacetylase H4K16 [8, 51]. The depletion of HDAC1 and HDAC2 have both been found to increase the levels of acetylated H4K16 [45, 51]. HDAC2 depletion has been shown to enhance memory, increase the number of synapses in the brain and does not affect the DNA damage response negatively [133]. However, the depletion of HDAC1 is associated with aberrant cell cycle activity and the accumulation of DSBs, so is too toxic for a beneficial treatment [134].

There is cell-selective toxicity in HDAC3 inhibition, where it is found to be toxic in mouse embryonic fibroblast cells but not overtly toxic in neurons [135, 136]. HDAC3 deficiency has been found to be neuroprotective towards low-potassium induced cell death and oxidative damage that occurs [135].

HDAC6 depletion has been found to rescue neurons from cell death and promotes their regeneration [137]. HDAC6 is relatively non-toxic and could

potentially be used as a therapeutic towards neurodegenerative diseases that occur in the CNS [137].

The use of a HDAC inhibitors has been shown to increase the HRR response, rescue cells from cell death, and promote their regeneration. A possible next step, after establishing if HRR can occur in N2a cells, could be to use a HDAC inhibitor in combination with *I-SceI* cleavage. This could increase the acetylation of H4K16 and the HRR pathway could potentially be amplified.

6.4 Other Post-Mitotic Cells

Cardiomyocytes are cells in the heart which, like neurons, are post-mitotic and not readily replaced if lost. It is believed that these cells also utilise the NHEJ pathway as the HRR pathway is limited to the S and G2 phase of the cell cycle [138]. However, as there is now evidence of RNA templated repair it could be possible that these cells repair themselves by HRR. There is also evidence that cardiomyocytes can be regenerated, at an extremely slow rate [138], which shows that these cells are capable of re-entering the cell cycle and means that HRR could also occur by this means.

In future experiments with N2a cells, if successful, it could provide evidence that HRR can occur in post-mitotic cells. This information could be beneficial, not just for neurological research but also for heart disease research.

References

1. Stuart, G., Spruston, N., and Häusser M, *Dendrites.* OUP Oxford, 2016.
2. Rutecki, P.A., *Neuronal excitability: voltage-dependent currents and synaptic transmission.* J Clin Neurophysiol, 1992. **9**(2): p. 195-211.
3. Bhatheja, K. and J. Field, *Schwann cells: origins and role in axonal maintenance and regeneration.* Int J Biochem Cell Biol, 2006. **38**(12): p. 1995-9.
4. Raz, A.a.P., M., *Central Nervous System Physiology: Neurophysiology*. Second Edition ed. Pharmacology and Physiology for Anesthesia, ed. H. Hemming. 103-122.
5. Farley, A., et al., *Nervous system: part 1.* Nurs Stand, 2014. **28**(31): p. 46-51.
6. 1080, D., Neuron description, *"Anatomy and Physiology" by the US National Cancer Institute's Surveillance, Epidemiology and End Results (SEER) Program* 2019.
7. Pan, L., J. Penney, and L.H. Tsai, *Chromatin regulation of DNA damage repair and genome integrity in the central nervous system.* J Mol Biol, 2014. **426**(20): p. 3376-88.
8. Brochier, C. and B. Langley, *Chromatin modifications associated with DNA double-strand breaks repair as potential targets for neurological diseases.* Neurotherapeutics, 2013. **10**(4): p. 817-30.
9. Keeney, S. and M.J. Neale, *Initiation of meiotic recombination by formation of DNA double-strand breaks: mechanism and regulation.* Biochem Soc Trans, 2006. **34**(Pt 4): p. 523-5.
10. Dudley, D.D., et al., *Mechanism and control of V(D)J recombination versus class switch recombination: similarities and differences.* Adv Immunol, 2005. **86**: p. 43-112.
11. Chapman, J.R., M.R. Taylor, and S.J. Boulton, *Playing the end game: DNA double-strand break repair pathway choice.* Mol Cell, 2012. **47**(4): p. 497-510.
12. Geacintov, N.E., et al., *NMR solution structures of stereoisometric covalent polycyclic aromatic carcinogen-DNA adduct: principles, patterns, and diversity.* Chem Res Toxicol, 1997. **10**(2): p. 111-46.
13. Veglia, F., G. Matullo, and P. Vineis, *Bulky DNA adducts and risk of cancer: a meta-analysis.* Cancer Epidemiol Biomarkers Prev, 2003. **12**(2): p. 157-60.
14. Deans, A.J. and S.C. West, *DNA interstrand crosslink repair and cancer.* Nat Rev Cancer, 2011. **11**(7): p. 467-80.
15. Krokan, H.E. and M. Bjoras, *Base excision repair.* Cold Spring Harb Perspect Biol, 2013. **5**(4): p. a012583.
16. Caldecott, K.W., *Single-strand break repair and genetic disease.* Nat Rev Genet, 2008. **9**(8): p. 619-31.
17. Khoronenkova, S.V. and G.L. Dianov, *ATM prevents DSB formation by coordinating SSB repair and cell cycle progression.* Proc Natl Acad Sci U S A, 2015. **112**(13): p. 3997-4002.

18. Meers, C., H. Keskin, and F. Storici, *DNA repair by RNA: Templated, or not templated, that is the question.* DNA Repair (Amst), 2016. **44**: p. 17-21.

19. Barzilai, A., S. Biton, and Y. Shiloh, *The role of the DNA damage response in neuronal development, organization and maintenance.* DNA Repair (Amst), 2008. **7**(7): p. 1010-27.

20. Pfeiffer, P., W. Goedecke, and G. Obe, *Mechanisms of DNA double-strand break repair and their potential to induce chromosomal aberrations.* Mutagenesis, 2000. **15**(4): p. 289-302.

21. Mathews, L.A., Cabarcas, Stephanie M., Hurt, Elaine (Eds.), *DNA repair of cancer stem cells*. 2013

22. Lindahl, T., *Instability and decay of the primary structure of DNA.* Nature, 1993. **362**(6422): p. 709-15.

23. Dianov, G. and T. Lindahl, *Reconstitution of the DNA base excision-repair pathway.* Curr Biol, 1994. **4**(12): p. 1069-76.

24. Iyer, R.R., et al., *DNA mismatch repair: functions and mechanisms.* Chem Rev, 2006. **106**(2): p. 302-23.

25. Lee, Y. and P.J. McKinnon, *Responding to DNA double strand breaks in the nervous system.* Neuroscience, 2007. **145**(4): p. 1365-74.

26. Lee, J.H. and T.T. Paull, *Activation and regulation of ATM kinase activity in response to DNA double-strand breaks.* Oncogene, 2007. **26**(56): p. 7741-8.

27. Kinner, A., et al., *Gamma-H2AX in recognition and signaling of DNA double-strand breaks in the context of chromatin.* Nucleic Acids Res, 2008. **36**(17): p. 5678-94.

28. Yoshiyama, K.O., K. Sakaguchi, and S. Kimura, *DNA damage response in plants: conserved and variable response compared to animals.* Biology (Basel), 2013. **2**(4): p. 1338-56.

29. Feng, L., et al., *Cell cycle-dependent inhibition of 53BP1 signaling by BRCA1.* Cell Discov, 2015. **1**: p. 15019.

30. White, R.R. and J. Vijg, *Do DNA Double-Strand Breaks Drive Aging?* Mol Cell, 2016. **63**(5): p. 729-38.

31. Thapar, R., *Regulation of DNA Double-Strand Break Repair by Non-Coding RNAs.* Molecules, 2018. **23**(11).

32. Brandsma, I. and D.C. Gent, *Pathway choice in DNA double strand break repair: observations of a balancing act.* Genome Integr, 2012. **3**(1): p. 9.

33. Sugiyama, T., E.M. Zaitseva, and S.C. Kowalczykowski, *A single-stranded DNA-binding protein is needed for efficient presynaptic complex formation by the Saccharomyces cerevisiae Rad51 protein.* J Biol Chem, 1997. **272**(12): p. 7940-5.

34. Wyman, C., D. Ristic, and R. Kanaar, *Homologous recombination-mediated double-strand break repair.* DNA Repair (Amst), 2004. **3**(8-9): p. 827-33.

35. Li, X. and W.D. Heyer, *Homologous recombination in DNA repair and DNA damage tolerance.* Cell Res, 2008. **18**(1): p. 99-113.

36. Lieber, M.R., *The mechanism of double-strand DNA break repair by the nonhomologous DNA end-joining pathway.* Annu Rev Biochem, 2010. **79**: p. 181-211.

37. Her, J. and S.F. Bunting, *How cells ensure correct repair of DNA double-strand breaks.* J Biol Chem, 2018. **293**(27): p. 10502-10511.

38. Doherty, A.J. and S.P. Jackson, *DNA repair: how Ku makes ends meet.* Curr Biol, 2001. **11**(22): p. R920-4.

39. Daley, J.M., et al., *DNA joint dependence of pol X family polymerase action in nonhomologous end joining.* J Biol Chem, 2005. **280**(32): p. 29030-7.

40. Wilson, T.E., U. Grawunder, and M.R. Lieber, *Yeast DNA ligase IV mediates non-homologous DNA end joining.* Nature, 1997. **388**(6641): p. 495-8.

41. Vilenchik, M.M. and A.G. Knudson, *Endogenous DNA double-strand breaks: production, fidelity of repair, and induction of cancer.* Proc Natl Acad Sci U S A, 2003. **100**(22): p. 12871-6.

42. Barzilai, A., *DNA damage, neuronal and glial cell death and neurodegeneration.* Apoptosis, 2010. **15**(11): p. 1371-81.

43. Bunting, S.F., et al., *53BP1 inhibits homologous recombination in Brca1-deficient cells by blocking resection of DNA breaks.* Cell, 2010. **141**(2): p. 243-54.

44. Wu, J. and M. Grunstein, *25 years after the nucleosome model: chromatin modifications.* Trends Biochem Sci, 2000. **25**(12): p. 619-23.

45. Tang, J., et al., *Acetylation limits 53BP1 association with damaged chromatin to promote homologous recombination.* Nat Struct Mol Biol, 2013. **20**(3): p. 317-25.

46. Van, H.T. and M.A. Santos, *Histone modifications and the DNA double-strand break response.* Cell Cycle, 2018. **17**(21-22): p. 2399-2410.

47. Masumoto, H., et al., *A role for cell-cycle-regulated histone H3 lysine 56 acetylation in the DNA damage response.* Nature, 2005. **436**(7048): p. 294-8.

48. Celic, I., et al., *The sirtuins hst3 and Hst4p preserve genome integrity by controlling histone h3 lysine 56 deacetylation.* Curr Biol, 2006. **16**(13): p. 1280-9.

49. Vempati, R.K., et al., *p300-mediated acetylation of histone H3 lysine 56 functions in DNA damage response in mammals.* J Biol Chem, 2010. **285**(37): p. 28553-64.

50. Das, C., et al., *CBP/p300-mediated acetylation of histone H3 on lysine 56.* Nature, 2009. **459**(7243): p. 113-7.

51. Miller, K.M., et al., *Human HDAC1 and HDAC2 function in the DNA-damage response to promote DNA nonhomologous end-joining.* Nat Struct Mol Biol, 2010. **17**(9): p. 1144-51.

52. Bakkenist, C.J. and M.B. Kastan, *DNA damage activates ATM through intermolecular autophosphorylation and dimer dissociation.* Nature, 2003. **421**(6922): p. 499-506.

53. Park, E.J., et al., *DNA-PK is activated by nucleosomes and phosphorylates H2AX within the nucleosomes in an acetylation-dependent manner.* Nucleic Acids Res, 2003. **31**(23): p. 6819-27.

54. Cook, P.J., et al., *Tyrosine dephosphorylation of H2AX modulates apoptosis and survival decisions.* Nature, 2009. **458**(7238): p. 591-6.

55. Xiao, A., et al., *WSTF regulates the H2A.X DNA damage response via a novel tyrosine kinase activity.* Nature, 2009. **457**(7225): p. 57-62.

56. Chowdhury, D., et al., *gamma-H2AX dephosphorylation by protein phosphatase 2A facilitates DNA double-strand break repair.* Mol Cell, 2005. **20**(5): p. 801-9.

57. Schwertman, P., S. Bekker-Jensen, and N. Mailand, *Regulation of DNA double-strand break repair by ubiquitin and ubiquitin-like modifiers.* Nat Rev Mol Cell Biol, 2016. **17**(6): p. 379-94.

58. Stucki, M., et al., *MDC1 directly binds phosphorylated histone H2AX to regulate cellular responses to DNA double-strand breaks.* Cell, 2005. **123**(7): p. 1213-26.

59. Lou, Z., et al., *MDC1 maintains genomic stability by participating in the amplification of ATM-dependent DNA damage signals.* Mol Cell, 2006. **21**(2): p. 187-200.

60. Mattiroli, F., et al., *RNF168 ubiquitinates K13-15 on H2A/H2AX to drive DNA damage signaling.* Cell, 2012. **150**(6): p. 1182-95.

61. Jorgensen, S., G. Schotta, and C.S. Sorensen, *Histone H4 lysine 20 methylation: key player in epigenetic regulation of genomic integrity.* Nucleic Acids Res, 2013. **41**(5): p. 2797-806.

62. Botuyan, M.V., et al., *Structural basis for the methylation state-specific recognition of histone H4-K20 by 53BP1 and Crb2 in DNA repair.* Cell, 2006. **127**(7): p. 1361-73.

63. Huyen, Y., et al., *Methylated lysine 79 of histone H3 targets 53BP1 to DNA double-strand breaks.* Nature, 2004. **432**(7015): p. 406-11.

64. Monks, T.J., et al., *Ros-induced histone modifications and their role in cell survival and cell death.* Drug Metab Rev, 2006. **38**(4): p. 755-67.

65. Wang, M., et al., *PARP-1 and Ku compete for repair of DNA double strand breaks by distinct NHEJ pathways.* Nucleic Acids Res, 2006. **34**(21): p. 6170-82.

66. Hoeijmakers, J.H., *DNA damage, aging, and cancer.* N Engl J Med, 2009. **361**(15): p. 1475-85.

67. Harman, D., *The aging process.* Proc Natl Acad Sci U S A, 1981. **78**(11): p. 7124-8.

68. Weissman, L., et al., *DNA repair, mitochondria, and neurodegeneration.* Neuroscience, 2007. **145**(4): p. 1318-29.

69. Yannone, S.M., et al., *Werner syndrome protein is regulated and phosphorylated by DNA-dependent protein kinase.* J Biol Chem, 2001. **276**(41): p. 38242-8.

70. Cooper, M.P., et al., *Ku complex interacts with and stimulates the Werner protein.* Genes Dev, 2000. **14**(8): p. 907-12.

71. Kusumoto, R., et al., *Werner protein cooperates with the XRCC4-DNA ligase IV complex in end-processing.* Biochemistry, 2008. **47**(28): p. 7548-56.

72. Cheng, W.H., et al., *Linkage between Werner syndrome protein and the Mre11 complex via Nbs1.* J Biol Chem, 2004. **279**(20): p. 21169-76.

73. Huang, S., et al., *The spectrum of WRN mutations in Werner syndrome patients.* Hum Mutat, 2006. **27**(6): p. 558-67.

74. Spillare, E.A., et al., *p53-mediated apoptosis is attenuated in Werner syndrome cells.* Genes Dev, 1999. **13**(11): p. 1355-60.

75. Muftuoglu, M., et al., *The clinical characteristics of Werner syndrome: molecular and biochemical diagnosis.* Hum Genet, 2008. **124**(4): p. 369-77.

76. Kakigi, R., et al., *Accelerated aging of the brain in Werner's syndrome.* Neurology, 1992. **42**(4): p. 922-4.

77. Peleg, S., et al., *Altered histone acetylation is associated with age-dependent memory impairment in mice.* Science, 2010. **328**(5979): p. 753-6.

78. Krishnan, V., et al., *Histone H4 lysine 16 hypoacetylation is associated with defective DNA repair and premature senescence in Zmpste24-deficient mice.* Proc Natl Acad Sci U S A, 2011. **108**(30): p. 12325-30.

79. Siddiqui, M.S., et al., *Persistent gammaH2AX: A promising molecular marker of DNA damage and aging.* Mutat Res Rev Mutat Res, 2015. **766**: p. 1-19.

80. Sedelnikova, O.A., et al., *Senescing human cells and ageing mice accumulate DNA lesions with unrepairable double-strand breaks.* Nat Cell Biol, 2004. **6**(2): p. 168-70.

81. Fumagalli, M., et al., *Telomeric DNA damage is irreparable and causes persistent DNA-damage-response activation.* Nat Cell Biol, 2012. **14**(4): p. 355-65.

82. Hewitt, G., et al., *Telomeres are favoured targets of a persistent DNA damage response in ageing and stress-induced senescence.* Nat Commun, 2012. **3**: p. 708.

83. Torudd, J., et al., *Dose-response for radiation-induced apoptosis, residual 53BP1 foci and DNA-loop relaxation in human lymphocytes.* Int J Radiat Biol, 2005. **81**(2): p. 125-38.

84. Sedelnikova, O.A., et al., *Delayed kinetics of DNA double-strand break processing in normal and pathological aging.* Aging Cell, 2008. **7**(1): p. 89-100.

85. Myung, N.H., et al., *Evidence of DNA damage in Alzheimer disease: phosphorylation of histone H2AX in astrocytes.* Age (Dordr), 2008. **30**(4): p. 209-15.

86. Coppede, F. and L. Migliore, *DNA damage in neurodegenerative diseases.* Mutat Res, 2015. **776**: p. 84-97.

87. Jeppesen, D.K., V.A. Bohr, and T. Stevnsner, *DNA repair deficiency in neurodegeneration.* Prog Neurobiol, 2011. **94**(2): p. 166-200.

88. Mullaart, E., et al., *Increased levels of DNA breaks in cerebral cortex of Alzheimer's disease patients.* Neurobiol Aging, 1990. **11**(3): p. 169-73.

89. Shackelford, D.A., *DNA end joining activity is reduced in Alzheimer's disease.* Neurobiol Aging, 2006. **27**(4): p. 596-605.

90. Jacobsen, E., et al., *Deficiency of the Mre11 DNA repair complex in Alzheimer's disease brains.* Brain Res Mol Brain Res, 2004. **128**(1): p. 1-7.

91. Suberbielle, E., et al., *Physiologic brain activity causes DNA double-strand breaks in neurons, with exacerbation by amyloid-beta.* Nat Neurosci, 2013. **16**(5): p. 613-21.

92. Mazzoni, P., B. Shabbott, and J.C. Cortes, *Motor control abnormalities in Parkinson's disease.* Cold Spring Harb Perspect Med, 2012. **2**(6): p. a009282.

93. Hegde, M.L., et al., *Studies on genomic DNA topology and stability in brain regions of Parkinson's disease.* Arch Biochem Biophys, 2006. **449**(1-2): p. 143-56.

94. Ravits, J., et al., *Deciphering amyotrophic lateral sclerosis: what phenotype, neuropathology and genetics are telling us about pathogenesis.* Amyotroph Lateral Scler Frontotemporal Degener, 2013. **14 Suppl 1**: p. 5-18.

95. Hardiman, O., et al., *Amyotrophic lateral sclerosis.* Nat Rev Dis Primers, 2017. **3**: p. 17071.

96. Hobson, E.V. and C.J. McDermott, *Supportive and symptomatic management of amyotrophic lateral sclerosis.* Nat Rev Neurol, 2016. **12**(9): p. 526-38.

97. Orrell, R.W., et al., *Clinical characteristics of SOD1 gene mutations in UK families with ALS.* J Neurol Sci, 1999. **169**(1-2): p. 56-60.

98. Martin, L.J., et al., *Motor neuron degeneration in amyotrophic lateral sclerosis mutant superoxide dismutase-1 transgenic mice: mechanisms of mitochondriopathy and cell death.* J Comp Neurol, 2007. **500**(1): p. 20-46.

99. Shaikh, A.Y. and L.J. Martin, *DNA base-excision repair enzyme apurinic/apyrimidinic endonuclease/redox factor-1 is increased and competent in the brain and spinal cord of individuals with amyotrophic lateral sclerosis.* Neuromolecular Med, 2002. **2**(1): p. 47-60.

100. Savitsky, K., et al., *A single ataxia telangiectasia gene with a product similar to PI-3 kinase.* Science, 1995. **268**(5218): p. 1749-53.

101. Chun, H.H. and R.A. Gatti, *Ataxia-telangiectasia, an evolving phenotype.* DNA Repair (Amst), 2004. **3**(8-9): p. 1187-96.

102. Peterson, R.D., et al., *Cancer susceptibility in ataxia-telangiectasia.* Leukemia, 1992. **6 Suppl 1**: p. 8-13.

103. Crawford, T.O., *Ataxia telangiectasia.* Semin Pediatr Neurol, 1998. **5**(4): p. 287-94.

104. Crawford, T.O., et al., *Survival probability in ataxia telangiectasia.* Arch Dis Child, 2006. **91**(7): p. 610-1.

105. Barlow, C., et al., *Atm-deficient mice: a paradigm of ataxia telangiectasia.* Cell, 1996. **86**(1): p. 159-71.

106. Stewart, G.S., et al., *The DNA double-strand break repair gene hMRE11 is mutated in individuals with an ataxia-telangiectasia-like disorder.* Cell, 1999. **99**(6): p. 577-87.

107. Taylor, A.M., A. Groom, and P.J. Byrd, *Ataxia-telangiectasia-like disorder (ATLD)-its clinical presentation and molecular basis.* DNA Repair (Amst), 2004. **3**(8-9): p. 1219-25.

108. Buis, J., et al., *Mre11 nuclease activity has essential roles in DNA repair and genomic stability distinct from ATM activation.* Cell, 2008. **135**(1): p. 85-96.

109. Carney, J.P., et al., *The hMre11/hRad50 protein complex and Nijmegen breakage syndrome: linkage of double-strand break repair to the cellular DNA damage response.* Cell, 1998. **93**(3): p. 477-86.

110. Marczak, H., et al., *Nijmegen Breakage Syndrome Complicated With Primary Pulmonary Granulomas.* Pediatrics, 2018. **142**(4).

111. Zhu, J., et al., *Targeted disruption of the Nijmegen breakage syndrome gene NBS1 leads to early embryonic lethality in mice.* Curr Biol, 2001. **11**(2): p. 105-9.

112. Waltes, R., et al., *Human RAD50 deficiency in a Nijmegen breakage syndrome-like disorder.* Am J Hum Genet, 2009. **84**(5): p. 605-16.

113. Tzur-Gilat, A., et al., *Studying the cerebellar DNA damage response in the tissue culture dish.* Mech Ageing Dev, 2013. **134**(10): p. 496-505.

114. Kass, E.M., et al., *Double-strand break repair by homologous recombination in primary mouse somatic cells requires BRCA1 but not the ATM kinase.* Proc Natl Acad Sci U S A, 2013. **110**(14): p. 5564-9.

115. Kumar, M. and A. Katyal, *Data on retinoic acid and reduced serum concentration induced differentiation of Neuro-2a neuroblastoma cells.* Data Brief, 2018. **21**: p. 2435-2440.

116. Absher, M., *Hemocytometer counting*, in *Tissue culture*. 1973, Elsevier. p. 395-397.

117. Tremblay, R.G., et al., *Differentiation of mouse Neuro 2A cells into dopamine neurons.* J Neurosci Methods, 2010. **186**(1): p. 60-7.

118. Namsi, A., et al., *Induction of Neuronal Differentiation of Murine N2a Cells by Two Polyphenols Present in the Mediterranean Diet Mimicking Neurotrophins Activities: Resveratrol and Apigenin.* Diseases, 2018. **6**(3).

119. Zeng, M. and J.N. Zhou, *Roles of autophagy and mTOR signaling in neuronal differentiation of mouse neuroblastoma cells.* Cell Signal, 2008. **20**(4): p. 659-65.

120. Walsh, P.S., D.A. Metzger, and R. Higushi, *Chelex 100 as a medium for simple extraction of DNA for PCR-based typing from forensic material. BioTechniques 10(4): 506-13 (April 1991).* Biotechniques, 2013. **54**(3): p. 134-9.

121. Esquenet, M., et al., *LNCaP prostatic adenocarcinoma cells derived from low and high passage numbers display divergent responses not only to androgens but also to retinoids.* J Steroid Biochem Mol Biol, 1997. **62**(5-6): p. 391-9.

122. Briske-Anderson, M.J., J.W. Finley, and S.M. Newman, *The influence of culture time and passage number on the morphological and physiological development of Caco-2 cells.* Proc Soc Exp Biol Med, 1997. **214**(3): p. 248-57.

123. Chang-Liu, C.M. and G.E. Woloschak, *Effect of passage number on cellular response to DNA-damaging agents: cell survival and gene expression.* Cancer Lett, 1997. **113**(1-2): p. 77-86.

124. Yu, H., T.J. Cook, and P.J. Sinko, *Evidence for diminished functional expression of intestinal transporters in Caco-2 cell monolayers at high passages.* Pharm Res, 1997. **14**(6): p. 757-62.

125. Wenger, S.L., et al., *Comparison of established cell lines at different passages by karyotype and comparative genomic hybridization.* Biosci Rep, 2004. **24**(6): p. 631-9.

126. Sambuy, Y., et al., *The Caco-2 cell line as a model of the intestinal barrier: influence of cell and culture-related factors on Caco-2 cell functional characteristics.* Cell Biol Toxicol, 2005. **21**(1): p. 1-26.

127. Yao, X., et al., *Homology-mediated end joining-based targeted integration using CRISPR/Cas9.* Cell Res, 2017. **27**(6): p. 801-814.

128. Gordon, J., S. Amini, and M.K. White, *General overview of neuronal cell culture.* Methods Mol Biol, 2013. **1078**: p. 1-8.

129. Sztuba-Solinska, J., et al., *RNA-RNA recombination in plant virus replication and evolution.* Annu Rev Phytopathol, 2011. **49**: p. 415-43.

130. Storici, F., et al., *RNA-templated DNA repair.* Nature, 2007. **447**(7142): p. 338-41.

131. Storici, F., *RNA-mediated DNA modifications and RNA-templated DNA repair.* Curr Opin Mol Ther, 2008. **10**(3): p. 224-30.

132. Keskin, H., et al., *Transcript-RNA-templated DNA recombination and repair.* Nature, 2014. **515**(7527): p. 436-9.

133. Graff, J., et al., *An epigenetic blockade of cognitive functions in the neurodegenerating brain.* Nature, 2012. **483**(7388): p. 222-6.

134. Kim, D., et al., *Deregulation of HDAC1 by p25/Cdk5 in neurotoxicity.* Neuron, 2008. **60**(5): p. 803-17.

135. Bardai, F.H. and S.R. D'Mello, *Selective toxicity by HDAC3 in neurons: regulation by Akt and GSK3beta.* J Neurosci, 2011. **31**(5): p. 1746-51.

136. Bhaskara, S., et al., *Hdac3 is essential for the maintenance of chromatin structure and genome stability.* Cancer Cell, 2010. **18**(5): p. 436-47.

137. Rivieccio, M.A., et al., *HDAC6 is a target for protection and regeneration following injury in the nervous system.* Proc Natl Acad Sci U S A, 2009. **106**(46): p. 19599-604.

138. Bergmann, O., et al., *Evidence for cardiomyocyte renewal in humans.* Science, 2009. **324**(5923): p. 98-102.